Chapter 4
Circularly Polarized Luminescence in Helicene and Helicenoid Derivatives

Jeanne Crassous

Abstract In this chapter, we discuss the circularly polarized luminescence (CPL) of helicene and helicenoid derivatives. The organic helicenic derivatives are classified according to the type of atom (heteroatom or carbon) incorporated within the helical backbone. Transition-metal complexes and chiroptical devices incorporating helicene derivatives and exhibiting CPL activity are also presented.

4.1 Introduction

Circularly polarized luminescence (CPL) is a fascinating property of many classes of chiral emissive molecules. The well-known luminescence dissymmetry factor (g_{lum}) as a measure of the degree of circular polarization of emitted light is defined as $g_{lum} = 2\Delta I/I = 2(I_L - I_R)/(I_L + I_R)$, where I_L and I_R denote the left- and right-handed circularly polarized emission intensities, respectively. Various types of chiral fluorescent conjugated organic molecules exhibiting CPL are known and generally possess g_{lum} values on the order of 10^{-4}–10^{-2} [1–6]. Among them, helicenes are a special class of chiral molecules which consist of n *ortho*-fused aromatic rings combining a helical topology with an extended π-conjugation [7–9]. Since the first preparation of enantioenriched helicenes in 1956 [10], their chirality has essentially been characterized through their very large optical rotation (OR) values, and their intense and characteristic electronic circular dichroism (ECD). In more rare cases, vibrational circular dichroism (VCD) and Raman optical activity (ROA) of helicenes have been measured. More recently, strong interest has grown on the elucidation of the chirality-related emission properties of helicenes. Indeed, helicene derivatives can be regarded as helically shaped polycyclic aromatic hydrocarbons (PAHs); they thus usually display organic semiconducting behavior and are efficient chiral emitters. With the development of circularly polarized emission techniques, the CPL

J. Crassous (✉)
Univ Rennes, CNRS, ISCR (Institut des Sciences Chimiques de Rennes) - UMR6226, Rennes, France
e-mail: jeanne.crassous@univ-rennes1.fr

T. Mori (ed.), *Circularly Polarized Luminescence of Isolated Small Organic Molecules*, https://doi.org/10.1007/978-981-15-2309-0_4

activity of helicenes and helicenoids is therefore being more and more investigated. In this chapter, we present the helicene derivatives that have shown to display CPL. Helically twisted acenes will not be considered here.

Theoretically, the luminescence dissymmetry factor g_{lum} for the electronic transition $i \rightarrow j$ can be expressed by the following equation: $g_{\mathrm{lum}} = 4\frac{\left|\boldsymbol{\mu}_{ij}\right| \cdot \left|\mathbf{m}_{ji}\right| \cdot \cos\theta\boldsymbol{\mu},\mathbf{m}}{\left|\boldsymbol{\mu}_{ij}\right|^2 + \left|\mathbf{m}_{ji}\right|^2}$, where $\boldsymbol{\mu}_{ij}$ and $\mathbf{m}_{ij}$ are, respectively, the electric and magnetic transition dipole moment vectors, while $\theta\boldsymbol{\mu},\mathbf{m}$ is the angle between them. In the case of an electronic transition, the $|\mathbf{m}_{ji}|$ term is usually small with respect to $|\boldsymbol{\mu}_{ij}|$ so the equation becomes $g_{\mathrm{lum}} = 4\frac{\left|\mathbf{m}_{ji}\right|}{\left|\boldsymbol{\mu}_{ij}\right|}\cos\,\theta\boldsymbol{\mu},\mathbf{m}$. High g_{lum} values are therefore usually obtained for magnetic dipole-allowed transitions. For this reason, CPL spectroscopy is widely applied to chiral lanthanide(III) complexes: the magnetically allowed intraconfigurational $f \rightarrow f$ transitions of lanthanide metal ions often provide extraordinary g_{lum} values [11]. In general, chiral organic π-conjugated systems display luminescence dissymmetry factors significantly lower than lanthanide(III) compounds, due to their electronic transitions with strong electric dipole character. However, their easy processability, the wide range of emission wavelengths accessible, and good quantum yields of fluorescence, together with their propensity to self-assemble into chiral supramolecules or aggregates makes chiral π-conjugated molecules appealing systems for improved materials with CPL activity [4] . Therefore, there is a growing interest in the investigation of the CPL properties of chiral π-conjugated systems.

In 2018, Mori et al. tried to see whether there was a correlation between excitation and emission dissymmetry factors; they examined the experimental ratio $g_{\mathrm{lum}}/g_{\mathrm{abs}}$ (where $g_{\mathrm{abs}} = \Delta\varepsilon/\varepsilon$) for a series of chiral organic emissive molecules among which helicenes. They found that this ratio significantly depended on the structure of the helicenic molecule and varied between 0.16 and 28 [12].

This chapter is structured via the different types of CPL-active helicene derivatives, i.e., the N-, O-, S-, B-, Si-, P-, and C-based helicenes and helicenoids, together with transition metal complexes of helicenes exhibiting CPL.

4.2 CPL-Active N-Containing Helicenes

4.2.1 Helicenic Bridged Triarylamines

In 2003, Venkataraman et al. described the preparation of helical triarylamines. These compounds were among the first helicenic structures displaying clear CPL-activity [13]. The two diastereomers of (*P,S*)-**1a** and (*M,S*)-**1b** displayed identical absorption spectra (Fig. 4.1a, b and Table 4.1) in the UV-vis region with maximum absorption and emission occurring at 434 nm and 453 nm, respectively. These pseudoenantiomeric compounds showed mirror-image ECD and CPL spectra, revealing that the (1*S*)-camphanate substituent had no influence on the

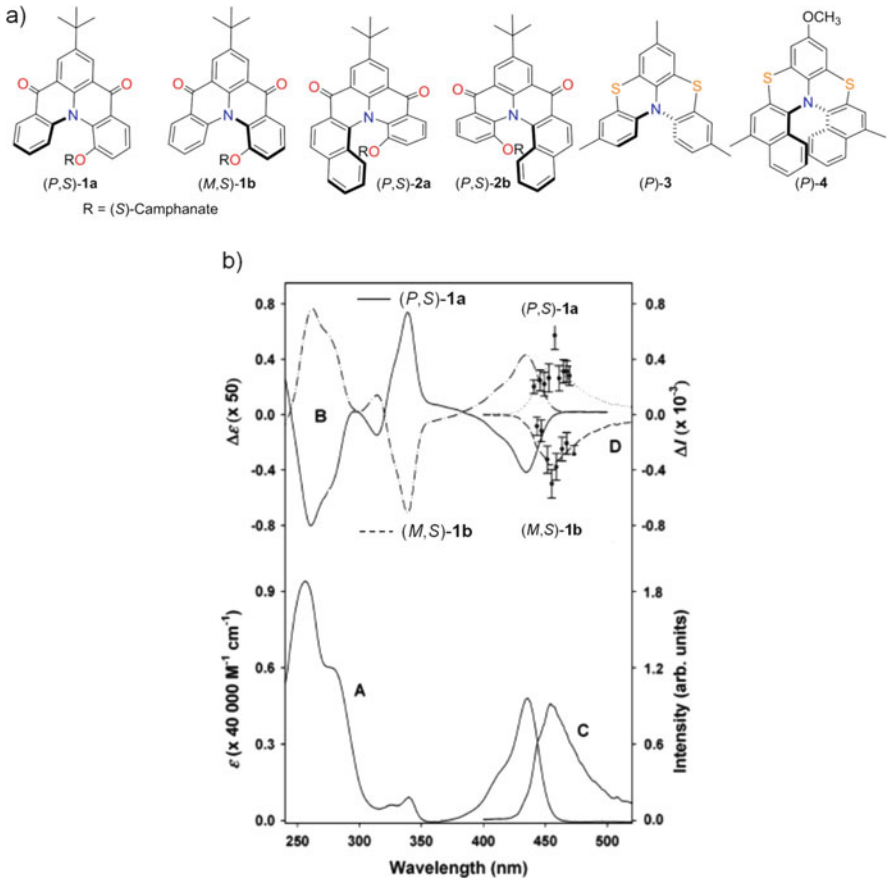

Fig. 4.1 (**a**) Chemical structures of helical bridged triarylamines **1a**,**b**; **2a**,**b;** and **3**–**4**. (**b**) UV-vis (A), ECD (B), fluorescence (C), and CPL (D) spectra of (*P,S*)-**1a** and (*M,S*)-**1b** in $CHCl_3$. Reproduced with permission [13]. Copyright 2003, American Chemical Society

chiroptical properties. Fluorescence dissymmetry factors of ±0.001 were obtained in chloroform. For the longer and more π-conjugated helicenes (*P,S*)-**2a** and (*M,S*)-**2b**, the maximum emission occurred at longer wavelength, i.e., 478 nm, and slightly smaller fluorescence dissymmetry factors (±0.0008) were obtained. For both compounds **1** and **2**, and for the same transition, g_{abs} and g_{lum} have essentially the same value showing no significant geometry change upon population of the emitting state. This is corroborated by the small Stokes shifts of the emission maxima. In 2016, the CPL activity of sulfurated systems **3** and **4** was measured by Longhi et al. [14] who found a g_{lum} as high 0.9×10^{-2} at ~510 nm (positive for (*M*) and vice versa, Table 4.1) for **4** while racemization was observed upon excitation of **3**. Post-functionalization of heterohelicene **5** with formyl (**6**) and diacyanovinyl (**7**) groups enabled to extend the π-conjugation [15]. The tails of UV-vis and ECD spectra together with emission and CPL bands in CH_2Cl_2 are highlighted in Fig. 4.2.

Table 4.1 Photophysical data of helical triarylamines and of azahelicenes

Compound	λ_{Abs} max [a] (nm)	λ_{Em} (nm)	Φ_F (%)	Solvent (CPL)	10^3 g_{abs}	10^3 g_{lum}	Ref.
(*P*,*S*)-**1a**	434	453	–	$CHCl_3$	+1.1	+0.9	[13]
(*M*,*S*)-**1b**	434	453	–	$CHCl_3$	−1.1	−1.1	[13]
(*P*,*S*)-**2a**	442	478	–	$CHCl_3$	+1.0	+0.8	[13]
(*M*,*S*)-**2b**	442	478	–	$CHCl_3$	−1.0	−0.7	[13]
(*M*)-**4**	400	510	1.6	$CHCl_3$	~7.3[b]	9	[14]
(*M*)-**5**	395	488	86	CH_2Cl_2	+5.6	+4.7	[15]
(*M*)-**6**	461	584	44	CH_2Cl_2	+2.1	+1.4	[15]
(*M*)-**7**	552	685	9	CH_2Cl_2	+0.9	+0.9	[15]
(*M*)-**8**	411	444	–	$CHCl_3$	+5.16	+5.9	[16]
(*M*)-**12**	381	467	5.1	$CHCl_3$	0.09[b]	<1	[17]
(*M*)-**13**	325	467	2.1	$CHCl_3$	0.02[b]	<1	[17]
(*P*)-**14**	442	477,509	1.4	$CHCl_3$	4.5	~0	[18]
(*P*,*P*)-**15**	448	471,492	19	$CHCl_3$	~1[b]	28 ± 2	[17]
(*P*,*P*)-**16**	445	454,480	9.4	$CHCl_3$	6.5	11 ± 2	[17]
(+)-**17**	416	473	39	CH_2Cl_2	~13[b]	9	[19]
(+)-**17**+TFA (200 eq.)	416	514	80	CH_2Cl_2	–	8	[19]

[a]Lowest-energy absorption band
[b]Taken from [12]

These compounds are strongly emissive, with quantum yields up to 0.86 for **5** in CH_2Cl_2 (Table 4.1). A clear red shift of absorption and emission was observed upon increasing the conjugation. The strong charge transfer and high polarity of these molecules were evidenced experimentally through the high solvent polarity dependence of the emission properties (emission wavelength and quantum yield). Regarding the chiroptics, similar g_{abs} and g_{lum} magnitudes were found for each compound with g_{abs}/g_{lum} of $+5.6 \times 10^{-3}/+4.7 \times 10^{-3}$ for (*M*)-**5**, $+2.1 \times 10^{-3}/+1.4 \times 10^{-3}$ for (*M*)-**6**, and $+ 0.9 \times 10^{-3}/+0.9 \times 10^{-3}$ for (*M*)-**7**. These properties were also compared in liquid state/solid state and in nanoparticles obtained by rapid precipitation in water. Respective g_{lum} values of 4.5×10^{-3}, 1.5×10^{-3}, and 2.8×10^{-3} were measured for nanoparticles of **5**, **6**, and **7** dispersed in water, showing that CPL activity was conserved. Note that the influence of solvent polarity was studied on the quantum yields but not on the absolute CPL values.

4.2.2 Emission Properties and CPL Activity of Azahelicenes

In 2014, Abbate et al. reported the CPL activity of blue-fluorescent 5-aza[6]helicene (**8**) enantiomers in relation to their ECD spectrum (Figs. 4.3 and 4.4) [20]. The sign of the CPL signal was controlled by the sign of the lower energy ECD named S-type

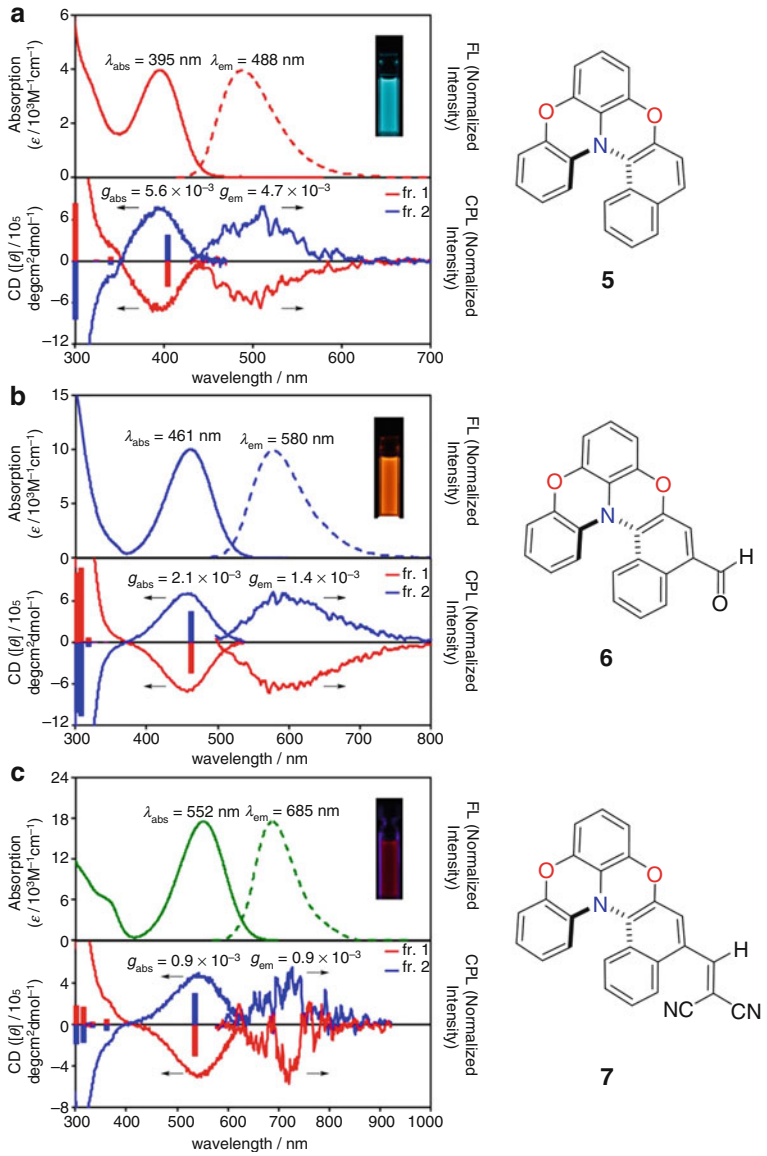

Fig. 4.2 UV-vis absorption (solid) and fluorescence (dashed) spectra (top) and CD and CPL spectra (bottom) for **5**, **6**, and **7** in CH_2Cl_2. The red and blue bars show the calculated ECD bands (CAM-B3LYP/6-31G(d)) for the (*P*)- and (*M*)-helices, respectively. The transition energies have been calibrated using a factor of 0.88. Photographs show the emission of **5**-**7**. Reproduced with permission [15]. Copyright 2017, American Chemical Society

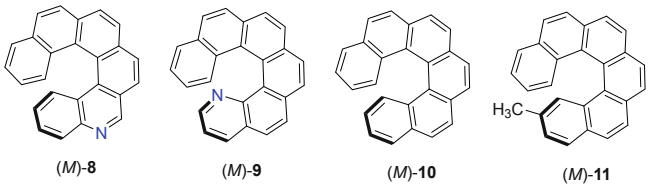

Fig. 4.3 Structures of aza[6]helicenes **8**,**9** and carbo[6]helicenes **10**,**11** [20, 21]

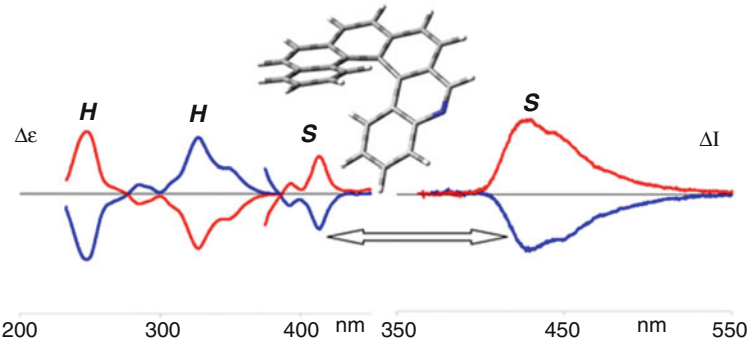

Fig. 4.4 ECD and CPL spectra of **8** in $CHCl_3$. Reproduced with permission [20]. Copyright 2014, American Chemical Society

band in relation with Inoue and Mori's nomenclature [22]. This effect was also shown in carbo[6]helicenes (*M*)-**10** and (*M*)-**11** which exhibited positive CPL signals at ~410 and 415 nm, respectively, in $CHCl_3$ (vide infra) [20]. In 2016, Longhi and Santoro reported the vibronically resolved calculated UV-vis, ECD, emission, and CPL spectra of **8**. A CPL dissymmetry factor g_{lum} of $+0.59 \times 10^{-3}$ at 444 nm was experimentally measured for (*M*)-**8** in $CHCl_3$ (Table 4.1) and used as a helically shaped chiral model to test the validity of advanced theoretical calculations of chiroptical techniques [16]. Note that the g_{lum} value of corresponding 1-aza[6]helicene **9** was evaluated to be between 10^{-4} and 10^{-3} by Fuchter, Campbell, and coworkers who used this helicene as a chiral inducer in organic light-emitting diodes (OLEDs, see Sect. 4.10) [21]

4.2.3 Double Vs. Single Azahelicenes

In 2014 Tanaka and coworkers reported the enantioselective synthesis of azahelicenes **12** and **13** and of S-shaped double azahelicenes **15** and **16** (Fig. 4.5) [17, 18]. Their photophysical properties are summarized in Table 4.1. Double azahelicenes **15** and **16** showed red shifts of absorption and emission maxima as compared with their corresponding single azahelicenes **12** and **13**. They also showed higher quantum yields in $CHCl_3$ solution. Interestingly, the CPL activity of

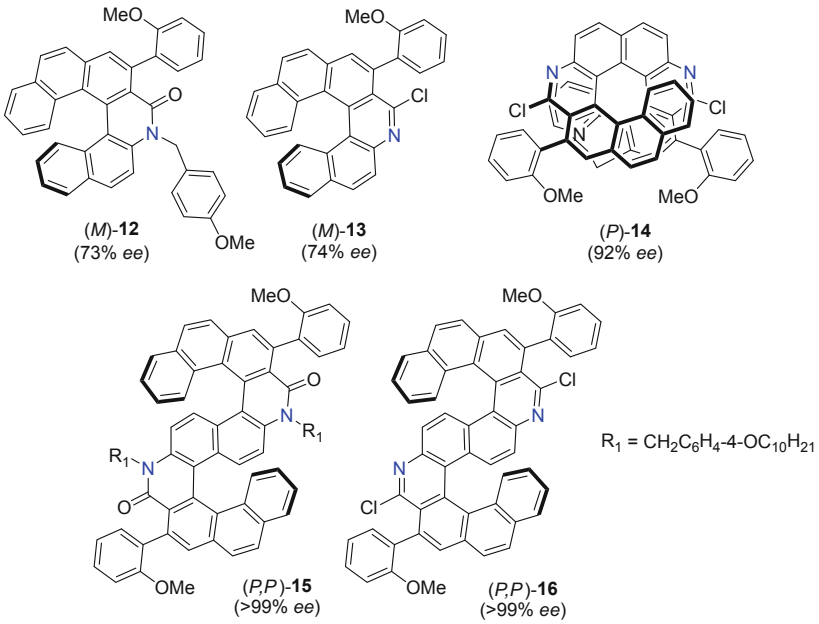

Fig. 4.5 Chemical structures of enantioenriched single aza[6]helicenes **12–14** and S-shaped double aza[6]helicenes **15**,**16** [17, 18]

the S-shaped double azahelicenes was significantly higher than that of the single azahelicenes. Indeed, CPL measurements showed intensities for azahelicenes **12** and **13** were below their measurable limit ($g_{lum} < 0.001$), whereas double azahelicenes **15** and **16** exhibited strong CPL activities, with $g_{lum} = 0.028$ at 492 nm for (+)-**15** and $g_{lum} = +0.011$ at 454 nm for (+)-**16** in $CHCl_3$ [17]. In 2016, (−) and (+)-aza[10]helicenes **14** were found to display $|g_{abs}| = 4.5 \times 10^{-3}$ at 303 nm which correspond to a smaller value than for *S*-shaped **16** ($|g_{abs}| = 6.5 \times 10^{-3}$ at 331 nm) but no CPL activity could be measured for **14** [18].

To explain the enhancement of CPL in S-shaped double helicenes, Mori et al. proposed in 2018 a protocol for rationally aligning multiple chiral units to boost the chiroptical responses, using hexahelicene **10** as a prototype [23]. To do so, they aligned two hexahelicenes in various orientations and examined by theoretical calculations which orientation resulted in the highest chiroptical performance from X-shaped or S-shaped double hexahelicenes (see Sect. 4.8.2).

4.2.4 Polyaza[7]helicenes

In 2017, Shibata et al. reported the synthesis of enantiopure polyaza[7]helicenes such as **17** (Fig. 4.6) possessing a 6-5-6-6-6-5-6 skeleton [19] which showed high fluorescence quantum yields under both neutral ($\Phi_F = 0.39$) and acidic conditions

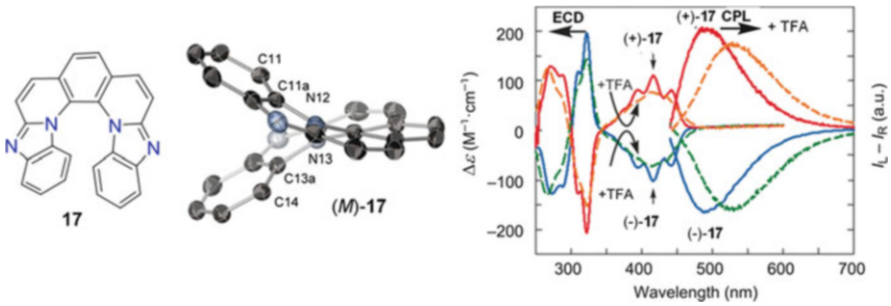

Fig. 4.6 Chemical structure, X-ray structure, ECD, and CPL spectra of neutral and acidic form of **17** enantiomers. Adapted with permission [19]. Copyright 2017, Wiley

($\Phi_F = 0.80$). The ECD spectrum of (+)-**17** showed several positive Cotton bands in the longer wavelength region with very similar shapes for both neutral and acidic forms. These observations imply that the electronic transitions have similar features in the ground state. Under both conditions, helicene **17** also shows strong CPL activity with a g_{lum} value under neutral conditions of 0.009 at 473 nm which is quite large for a heptahelicene derivative. Upon addition of 200 equivalent amounts of TFA, the g_{lum} value remained high (0.008 at 514 nm). Overall, these systems combine both high g_{lum} value with high quantum yields.

4.2.5 Azahelicenes with Fused Carbazole Cycles (Pyrrolohelicenes)

Pyrrole-incorporating PHAs have been shown to possess remarkable physical properties such as effective hole-transporting ability and bright emission. In 2012, Hiroto et al. reported pyrrole-fused system **18** displaying an aza[5]helicenic structure with a stable helical conformation, thanks to the presence of bulky ethynylsilylated groups (Fig. 4.7) [24]. Good fluorescence quantum yields were obtained for **18** ($\Phi_F = 0.36$) with a Stokes shift of 2220 cm^{-1} reflecting the distorted conformation of **18**; a CPL anisotropy factor $|g_{lum}|$ of 3×10^{-3} was measured for both enantiomers. The corresponding bis-butadiyne bridged azahelicene dimer (*M*,*M*)- and (*P*,*P*)-**20** with a figure-eight shape was prepared and exhibited red-shifted absorption and emission, with a higher fluorescence quantum yield ($\Phi_F = 0.55$) and higher g_{abs} and g_{lum} values as compared to (*M*)- and (*P*)-**18** (with opposite signs, see Table 4.2). This enhancement was attributed to the rigid conformation of the dimer [25]. See Sect. 4.3 for the corresponding CPL-active oxygen-containing helicene derivative **19**.

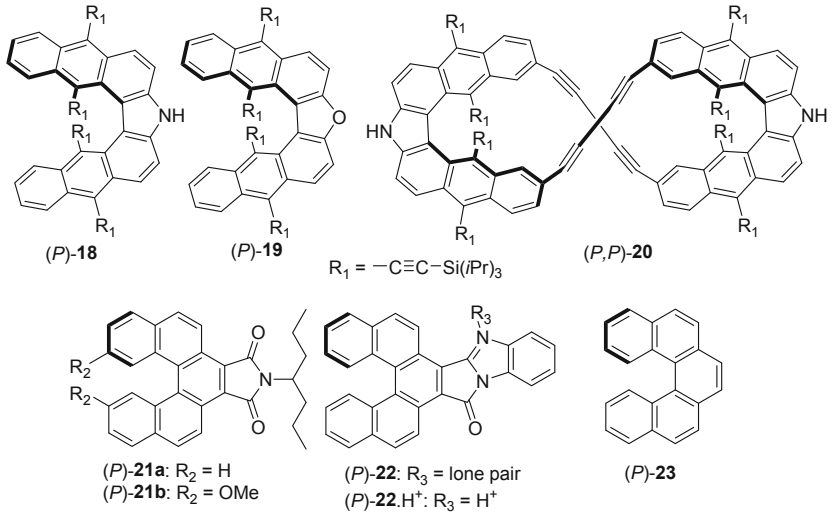

Fig. 4.7 Chemical structures of pentahelicenes incorporating a carbazole (**18**) together with a dimer (**20**) and a dibenzofurane analogue (**19**); pentahelicenes including imide functions (**21a**,**b** and **22**, **22**.H^+) together with pentacarbohelicene **23**

Table 4.2 Photophysical data of helicenes fused with pyrroles or imide cycles

Compound	$\lambda_{Abs}^{max\ a}$ (nm)	λ_{Em} (nm)	Φ_F (%)	Solvent (CPL)	10^3 g_{abs}	10^3 g_{lum}	Ref.
(*P*)-(+)-**18**	503	560	36	CH_2Cl_2	+1.4[b]	+3	[24]
(*P*,*P*)-(+)-**20**	526	588	55	CH_2Cl_2	−8.5	−8.5	[25]
(*P*)-(+)-**21a**	456	~480	37	THF	−4.8	−2.4	[26]
(*P*)-(+)-**21b**	475	~525	22	THF	−5.7	−2.3	[26]
(*P*)-(+)-**22**	450	575	6	CH_2Cl_2	–	−9.45	[27]
(*P*)-(+)-**22**.H^+	570	650	6	CH_2Cl_2	–	−5.92	[27]
(*P*)-(−)-**24a**	366	445	12.8	THF	−1.55	−1.2	[28]
(*P*)-(−)-**24b**	366	457	19.2	THF	−1.33	−1.5	[28]
(*P*)-(−)-**24c**	371	482	64.8	THF	−1.35	−0.8	[28]
(*P*)-(−)-**24d**	387	556	40.3	THF	−1.31	−0.8	[28]
(*P*)-(−)-**24e**	415	617	7.4	THF	−3.53	−0.2	[28]

[a]Lowest-energy absorption band
[b]Taken from [12]

4.2.6 Helicene Imide Derivatives

Aromatic diimides are known to display bright emission properties. In 2016, Hasobe and coworkers reported [5]carbohelicene derivatives **21a**,**b** fused with an electron-withdrawing maleimide and substituted with electron-donating methoxy

groups [26]. Compared to pristine [5]carbohelicene **23**, the introduction of an electron-withdrawing maleimide group onto a [5]carbohelicene core contributes to the stabilization of the LUMO level in **21a,** whereas the energy level of HOMO level in MeO-substituted **21b** increases due to the electron donation. As a result, the HOMO-LUMO gap of **21b** is smaller than that of **21a** and of carbo[5]helicene **23**, giving bathochromic shift of absorption and emission bands. The absolute fluorescence quantum yield of **21a** was found higher (0.37) as compared to [5] carbohelicene **23** (0.04), whereas Φ_F of **21b** was slightly smaller (0.22). The chirality of these [5]carbohelicene derivatives **21a**,**b** was evidenced by their ECD and CPL activities. In particular, **21a** and **21b** gave good CPL activity with anisotropy factors g_{lum} estimated to be $\pm 2.4 \times 10^{-3}$ and $\pm\ 2.3 \times 10^{-3}$ in THF. This example was the first observation of CPL in [5]carbohelicene derivatives which are usually thought to be configurationally unstable. Here, the authors verified that the CPL signal was stable with time in solution. Note that this negative CPL signal for the (*P*)-(+) isomer is a S-type one (vide supra and [22]), i.e. corresponding to the small negative ECD signal at 435 nm with g_{abs} values of $-4.8/-5.7 \times 10^{-3}$ for (*P*)-(+)-**21a/b**. The same authors also reported a carbo[5]helicene **22** bearing a fused benzimidazole and its protonated form **22**.H^+ (see Fig. 4.7 and Table 4.2) [27].

In 2016, Chen and coworkers reported the preparation of configurationally stable helical aromatic imides displaying full-color CPL responses [28]. For this purpose, they prepared enantiomers (*P*)-(−)- and (*M*)-(+)-**24a**-**e** with high *ee*'s (98.4–99%). Each pair of enantiomers displayed mirror-image ECD spectra of moderate magnitude and absolute configurations opposite to those of classical heterohelicenes. (*P*)-(−)- and (*M*)-(+)-**24a**-**e** exhibited full color fluorescence emission (from 445 to 617 nm) and mirror-image CPL signals in THF (Fig. 4.8). The g_{abs} values of the enantiomers fell within the range of $\pm 1.5 \times 10^{-3}$ to $\pm 3.5 \times 10^{-4}$ and the g_{lum} values between $\pm 0.2 \times 10^{-3}$ and $\pm\ 1.5 \times 10^{-3}$ (Table 4.2).

4.2.7 Carbocationic Azahelicenes

Lacour and coworkers prepared functionalized carbocationic [4]helicene (**25–30**) and [6]helicene (**31–33**) derivatives and studied their photophysical and chiroptical properties (Figs. 4.9 and 4.10 and Table 4.3) [29–31]. Interestingly, these compounds exhibit fluorescence emissions in the red to near infrared region (with Φ_F ranging from 0.01 to 0.445), which corresponds to an unusual spectral range for helicene-based chromophores, especially for fully organic ones. As a result, these helical derivatives may be interesting for chiral bioimaging. The same authors investigated different diaza[4]helicenium chiral dyes functionalized with different donor and acceptor groups in order to tune their chiroptical properties in terms of ECD and CPL responses (Fig. 4.9) [29]. These helical derivatives present ECD signatures up to 750 nm with moderate intensity in the visible-red region ($\Delta\varepsilon \sim 10\ M^{-1}\ cm^{-1}$), resulting from partial charge-transfer transitions involving the nitrogen atoms and the central carbocation. Furthermore, CPL

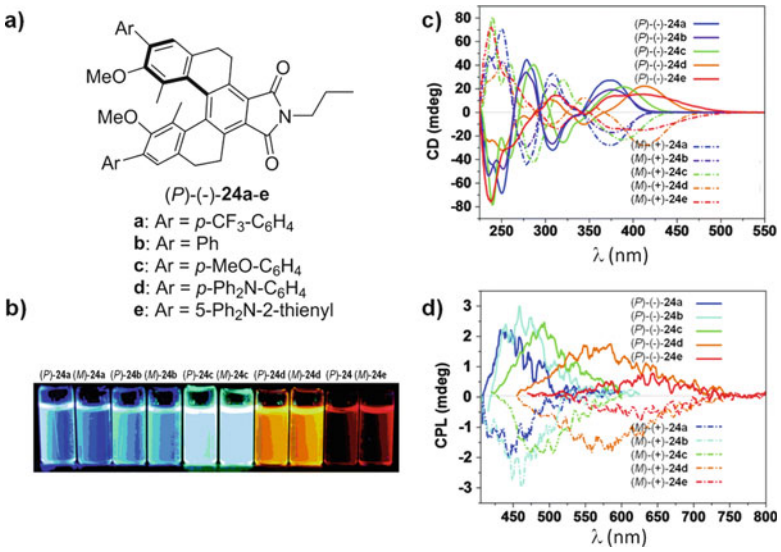

Fig. 4.8 (**a**) Chemical structure of **24a-e** ((*P*)-(−) enantiomers); (**b**) emission color panel of **24a-e**. (**c**) ECD spectra in THF of pure enantiomers. (**d**) CPL spectra in THF of pure enantiomers. Adapted with permission [28]. Copyright 2016, Royal Society of Chemistry

emissions were recorded between 650 and 700 nm and were characterized by a g_{lum} of ~10^{-4} to 10^{-3}. Such cationic chiral dyes were also used as pH-triggered ECD and CPL chiroptical switches when they possessed pH-sensitive group such as carboxylic acid. For instance, zwitterionic [4]helicene **29** was reported in 2016 as a reversible pH-triggered ECD/CPL chiroptical switch (Fig. 4.10) [30]. Protonated **30** displayed g_{lum} of around 5×10^{-4} and of similar order as g_{abs} (4×10^{-4}), while the carboxylate derivative **29** displayed no CPL, probably due to very low emission. Overall it represented an on-off CPL switch. Similarly, longer O-containing and N-containing [6]helicenium derivatives **31**–**33** displayed CPL signals (with opposite signs compared to their optical rotation values) with $|g_{lum}|$ between 0.32×10^{-3} and 2.1×10^{-3} in the infrared region [31].

4.3 CPL-Active Oxygen-Containing Helicene Derivatives

In 2011, Tanaka et al. reported a phthalhydrazide-functionalized [7]oxahelicene derivative **34** (Fig. 4.11), displaying a strong increase of g_{lum}, i.e., one order of magnitude, as compared to other helicenic derivatives [32]. This strong CPL enhancement was attributed to the presence of multiple-hydrogen-bonding sites enabling the formation of a trimeric structure which further organizes into chiral fibers (Fig. 4.12). These chiral fibers were 200 nm wide and 3–4 μm long in chloroform solutions, as characterized by SEM and AFM images. While UV-vis

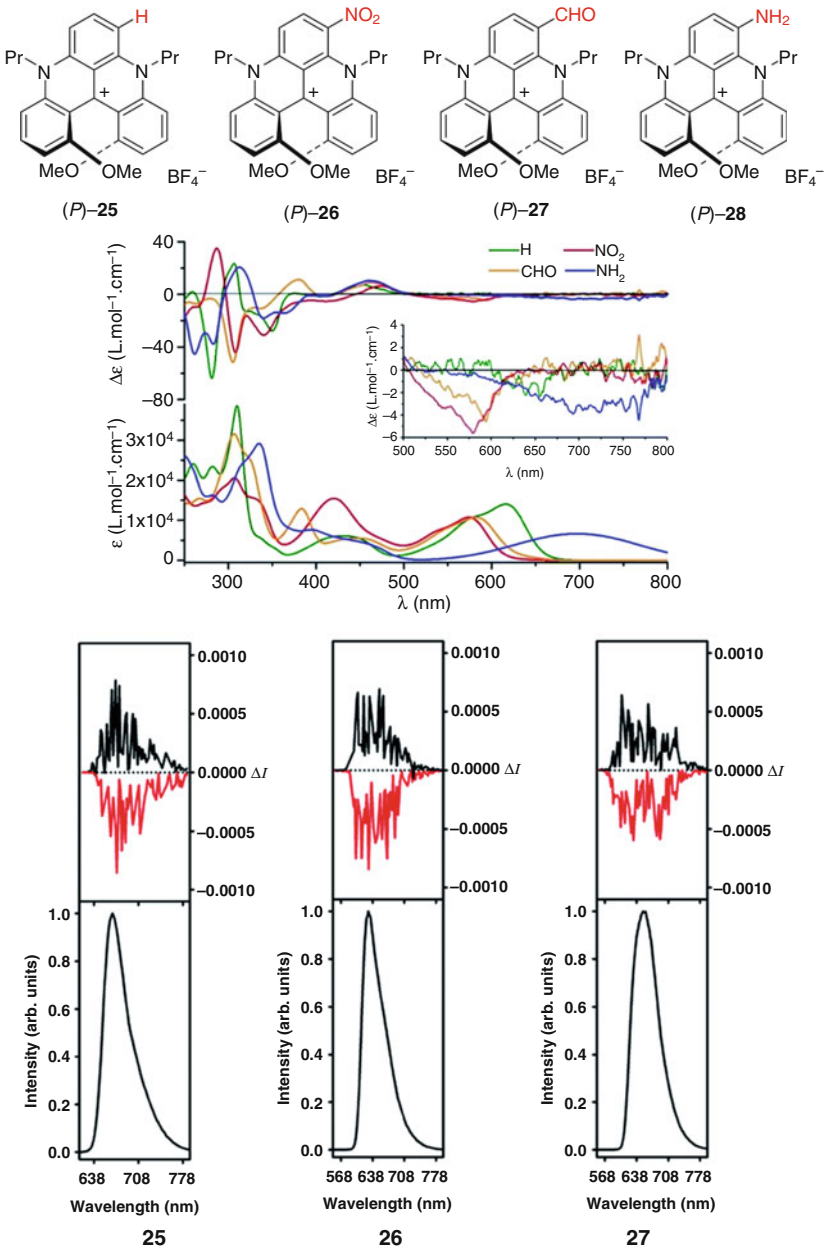

Fig. 4.9 Chemical structures of carbocationic diaza[4]helicenes **25–28** and their UV-vis, ECD and CPL activities. Adapted with permission [29]. Copyright 2016, Royal Society of Chemistry

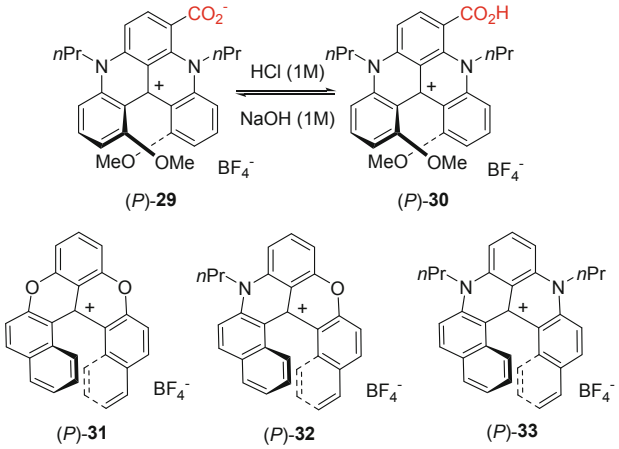

Fig. 4.10 Chemical structures of carbocationic diaza[4]helicenes **29–30** (pH-triggered switch) and O,N-containing carbocationic [6]helicenes [30, 31]

Table 4.3 Photophysical data of carbocationic azahelicenes

Compound	$\lambda_{Abs}^{max\ a}$ (nm)	λ_{Em} (nm)	Φ_F (%)	Solvent (CPL)	10^3 g_{abs}	10^3 g_{lum}	Ref.
(*P*)-(+)-**25**	616	667	13 (CH_3CN)	CH_2Cl_2	+0.15	+1.3	[29]
(*P*)-(+)-**26**	575	624	35 (CH_3CN)	CH_2Cl_2	+0.45	+1.6	[29]
(*P*)-(+)-**27**	582	640	37 (CH_3CN)	CH_2Cl_2	+0.36	+0.9	[29]
(*P*)-(+)-**29**	626	709	1	CH_3CN	~0.4	0	[30]
(*P*)-(+)-**30**	590	654	29	CH_3CN	0.4	0.5	[30]
(*P*)-(+)-**31**	562	595	44.5	CH_2Cl_2	−0.86[b]	−0.32	[31]
(*P*)-(+)-**32**	562	614	28	CH_2Cl_2	−1.3[b]	−2.1	[31]
(*P*)-(+)-**33**	614	658	28.4	CH_2Cl_2	−0.57[b]	−1.2	[31]

[a]Lowest-energy absorption band
[b]Taken from [12]

and ECD spectra seemed hardly sensitive to the formation of such aggregates, CPL measurements of **34** afforded g_{lum} of −0.035 for the (*M*) enantiomer in chloroform solutions, which was larger than in methanol solutions (−0.021). Similar systems, namely, [7]oxahelicene **35** (71% *ee*) and [9]oxahelicene derivative **36** (88% *ee*) were reported in 2017 [33]. Comparison of the photophysical data of these 9-oxahelicene **36** compared to **35** shows a redshift of both the absorption and luminescence spectra by ~20 to 50 nm, along with a decrease in fluorescence quantum yield (0.23–0.18). ECD and CPL spectra followed the same trend as for unpolarized UV-vis and fluorescence measurements, but with more intense ECD and CPL signals for **36**. Here the g_{lum} values around 10^{-3} in chloroform are classical for helicenic solutions

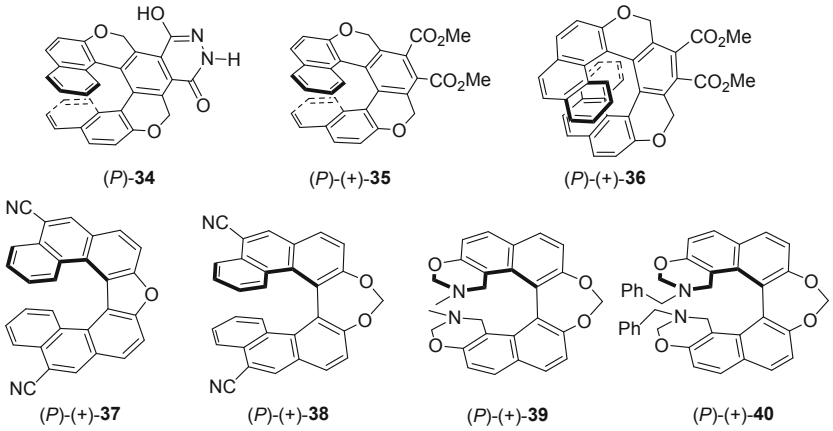

Fig. 4.11 Chemical structures of oxahelicenic derivatives

(see Table 4.4). Similarly to **18** (see Fig. 4.7), Hiroto and coworkers prepared *P*-(+) and *M*-(−) enantiomers of **19** which displayed strong orange fluorescence ($\Phi_F = 0.66$ in dichloromethane) and moderate CPL activity ($\pm 1.2 \times 10^{-3}$) [34]. Note that different emission properties between racemic and pure enantiomers were obtained for this compound in the solid state but no CPL in the solid state was reported.

In 2018, Bedekar and coworkers reported the preparation of (*P*)-(+) and (*M*)-(−) enantiomers of two 5,13-dicyano-9-oxa[7]helicene derivatives **37** and **38** and reported their photophysical and chiroptical properties [35]. These helical compounds are also active in CPL and mirror-like CPL spectra were measured with positive sign for (*P*) enantiomers, and g_{lum} values of 3–5 $\times$ 10^{-3} in DMSO solutions, i.e., falling within the classical range of helicene compounds. In 2014, Bedekar and coworkers also reported helicene-like bis-oxazines **39** and **40** from atropisomeric 7,7′-dihydroxy BINOL derivatives displaying good CPL activity, with g_{lum} of +0.0015/−0.0009 and + 0.0014/−0.0013 for (*P*)−/(*M*)-**39** and (*P*)−/(*M*)-**40**, respectively [36].

4.4 CPL-Active Sulfur-Containing Helicene Derivatives

There are few examples of CPL-active sulfur containing helicenes and helicenoids reported in the literature. First of all, it is worth to compare results obtained for **34** with those reported by Katz and coworkers in 2001 on thia[7]helicene-bisquinone derivative **41** decorated with four dodecyloxy groups [37]. Indeed, enantiopure [7] helicene **41** aggregated into columnar structures depending on the solvent type. The aggregation occurred in dodecane and in pure materials, but not in chloroform. The specific rotation showed strong enhancement with increasing concentration, i.e., $[\alpha]_D = 2800$ and 10,400 at 2×10^{-5} M and 2×10^{-2} M, respectively, in

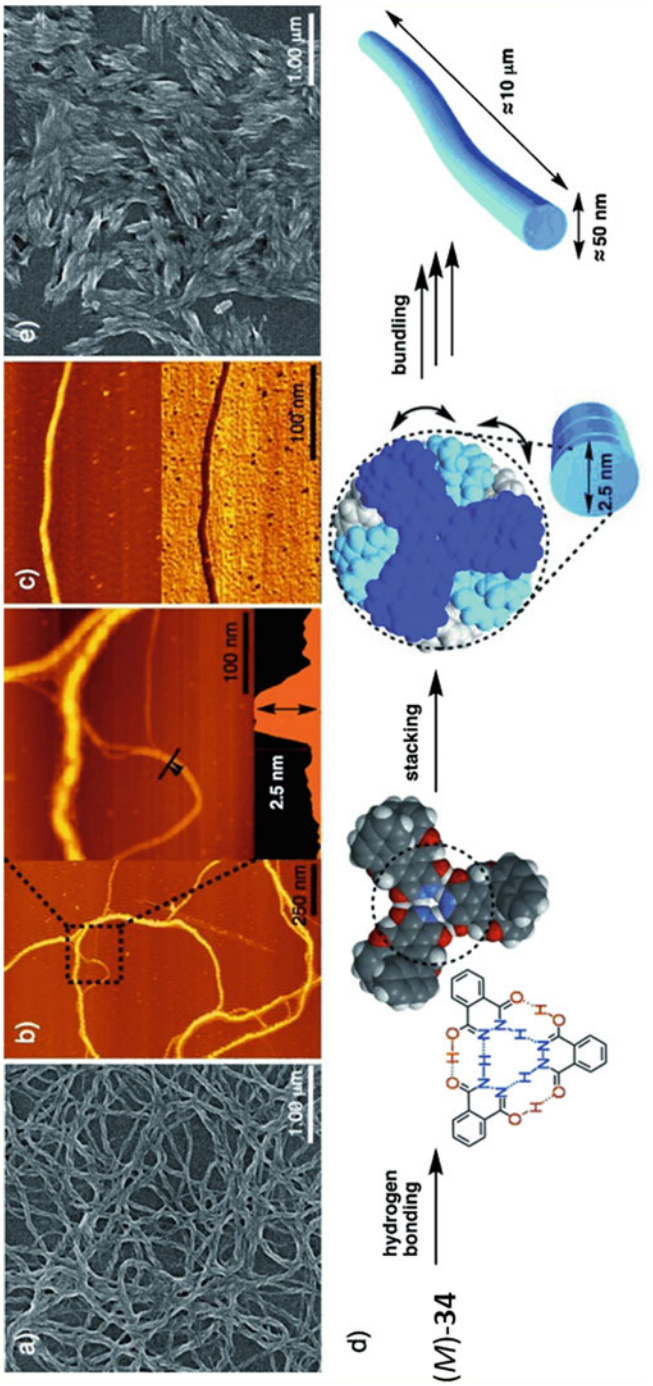

Fig. 4.12 AFM (**b**, **c**) and SEM images of (*M*)-**34** (**a**) and (*rac*)-**34** (**e**) prepared in toluene solutions. (**d**) Postulated mechanism for the formation of supramolecular chiral aggregates from a trimeric association. Reproduced with permission [32]. Copyright 2011, Wiley

Table 4.4 Photophysical data of oxahelicenic derivatives

Compound	λ_{Abs} $^{max\ a}$ (nm)	λ_{Em} (nm)	Φ_F (%)	Solvent (CPL)	$10^3\ g_{abs}$	$10^3\ g_{lum}$	Ref.
(*M*)-**34**	400	476	–	$CHCl_3$	−0.22[b]	−35	[32]
				MeOH	–	−21	[32]
(*P*)-(+)-**35**	380	479	23	$CHCl_3$	+0.56[b]	+0.95	[33]
(*P*)-(+)-**36**	388	514	18	$CHCl_3$	+1.3[b]	+1.1	[33]
(*P*)-**19**	500	550	66	CH_2Cl_2	-1.1[b]	−1.2	[34]
(*P*)-(+)-**37**	323	421	–	DMSO	–	3	[35]
(*P*)-(+)-**38**	310	439	–	DMSO	–	5	[35]
(*P*)-(+)-**39**	~360	430	–	CH_3CN	~+1.2[b]	+1.5	[36]
(*P*)-(+)-**40**	~360	430	–	CH_3CN	~+1.2[b]	+1.4	[36]

[a]Lowest-energy absorption band
[b]Taken form [12]

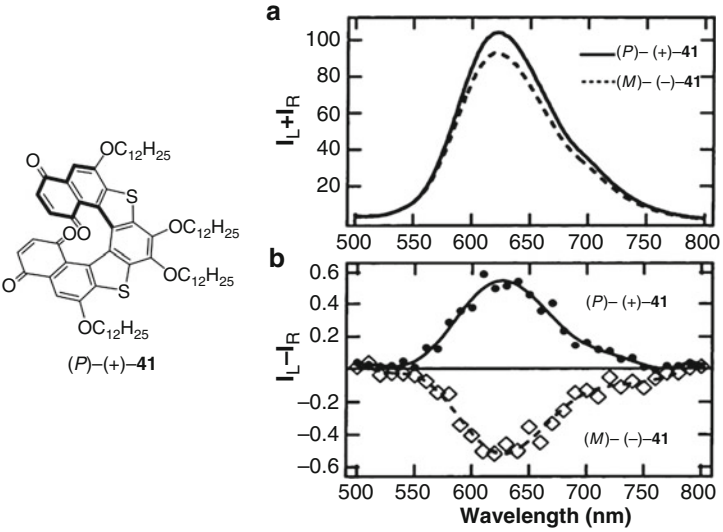

Fig. 4.13 Chemical structure of (*P*)-**41**. (**a**) Total luminescence and (**b**) CPL from solutions at 23 °C of (*P*)-(+) and (*M*)-(−)-**41** in dodecane (1×10^{-3} M) after excitation with unpolarized light ($\lambda_{ex} = 325$ nm). Adapted with permission [37]. Copyright 2001, American Chemical Society

dodecane. The same behavior was observed by ECD spectroscopy showing significant change for concentrated solutions in dodecane and for films obtained by drop casting from nonane solutions. Interestingly, for a concentration higher than 2×10^{-3} M, the solution was viscous and at 0.05 M it became a gel. CPL measurement was carried out for a solution with 1×10^{-3} M in dodecane (Fig. 4.13). Emission from enantiomer aggregates between 600 and 700 nm was found to be mirror image for enantiomeric systems. Interestingly, aggregation offered a strong dissymmetry factor ($g_{lum} = 0.01$ at around 630 nm). Likewise, the g_{abs} was large ($g_{abs} = 0.01$ between 500 and 550 nm); thus, the good similarity

suggests that the aggregates adopt the same chiral geometry in the ground and the excited states. However, the increased ordering of these aggregates also resulted in a large degree of linear polarization ($P = 0.39$) which can greatly affect the CPL measurement [38].

In 2016, Yamamoto et al. reported the synthesis of tetrasulfone[9]helicene **43** via the oxidation of tetrathia[9]helicene **42** [39]. Remarkably, it was found that the quantum yield of fluorescence for sulfone[9]helicene **43** ($\Phi_F = 0.27$) was ten times higher than tetrathia[9]helicene precursor **42** ($\Phi_F = 0.03$). The author explain this strong enhancement by a significant increase of the energy gap between the lowest singlet (S_1) and the triplet (T_1) excited states ΔE_{ST} in the case of **43** ($\Delta E_{ST} = 1.02$ eV) compared to ($\Delta E_{ST} = 0.60$ eV) for **42**, which may efficiently decrease the intersystem crossing (ISC) rate. Additionally, ECD spectra for **43** were recorded and an anisotropy factor $g_{abs} = -4.7 \times 10^{-3}$ was measured for the (*P*) enantiomer. Likewise, plotting the fluorescence CPL mirror-image spectra **43** enantiomers gave an estimated anisotropy factor value of $g_{lum} = -8.3 \times 10^{-4}$ for the (*P*)-**43** (Fig. 4.14).

A series of fluorescent "push-pull" tetrathia[9]helicenes based on quinoxaline (acceptor) fused with tetrathia[9]helicene (donor) derivatives was synthesized for control of the excited-state dynamics and circularly polarized luminescence (CPL) properties [40]. Introduction of a quinoxaline onto the tetrathia[9]helicene skeleton induced a "push-pull" character, which was enhanced by further introduction of electron-releasing or electron-withdrawing groups onto the quinoxaline unit (Fig. 4.15). Significant enhancement in the fluorescence quantum yields (Φ_F) was, for instance, obtained for **44**: ($\Phi_F = 0.30$, Table 4.5), which is more than 20 times

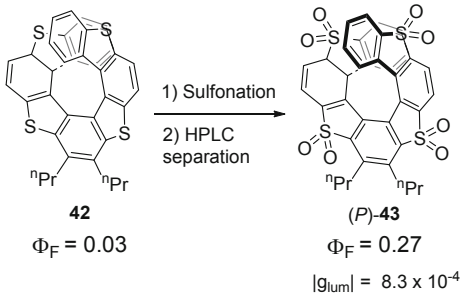

Fig. 4.14 Chemical structures of **42** and **43** and their emission data

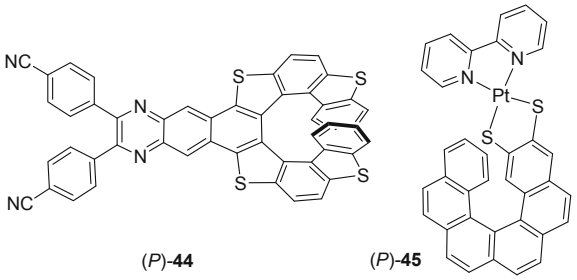

Fig. 4.15 Chemical structures of push-pull systems with improved luminescence and CPL emission and of a [6] helicene Pt(diimine) (dithiolene) complex

Table 4.5 Photophysical data of thiahelicenic derivatives

Compound	λ_{Abs} max a (nm)	λ_{Em} (nm)	Φ_F (%)	Solvent (CPL)	10^3 g_{abs}	10^3 g_{lum}	Ref.
(*P*)-(+)-**41**	470	630	–	Dodecane	+10	+10	[37]
(*P*)-**43**	390	450	27	THF	−4.7	−0.83	[39]
(*P*)-**44**	475	600	30	THF	+6.8	+3.0	[40]
(*P*)-**45**	562	715	15	CH_3CN	~+0.91[b]	+0.3	[41]

[a]Lowest-energy absorption band
[b]Taken form [12]

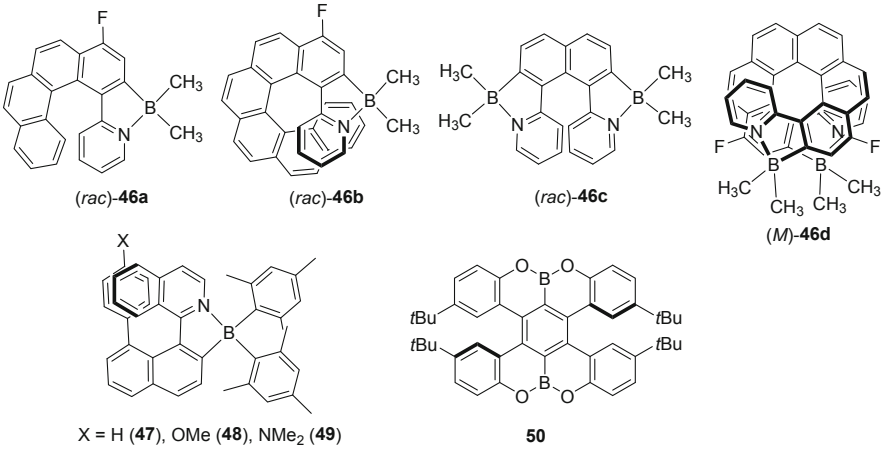

Fig. 4.16 Chemical structures of azabora[*n*]helicenes **46a–d** and **47–49** and oxaborahelicene **50**

larger than that of pristine tetrathia[9]helicene ($\Phi_F = 0.02$). Good CPL properties, with an anisotropy factor g_{lum} of 3.0×10^{-3} were measured for **44**. In 2017, Avarvari et al. reported the synthesis of (*P*) and (*M*)-**45**, corresponding to Pt(diimine)(dithiolene) connected with a [6]helicene unit [41]. Interestingly, (*P*) and (*M*)-**45** showed triplet state CPL activity at room temperature with low g_{lum} values of 3×10^{-4}.

4.5 CPL-Active Borahelicenes

Due to the electron-accepting and Lewis acidic character of boron, introducing one or several boron atoms into carbohelicenes generally results in strongly blue-emitting fluorophores. For chemical stability reasons, helicenes incorporating boron atoms are azaborahelicenes and oxaborahelicenes, i.e., also including N or O atoms. In 2017, our group prepared enantiopure azabora[n]helicenes **46a-d** incorporating one or two boron atoms and with 6,8 or 10 *ortho*-fused rings ($n = 6$, 8, 10, Fig. 4.16) [42]. These compounds displayed strong absorption between 250 and 450 nm

and blue fluorescence (λ_{Em} ~ 420–450 nm) with rather strong quantum yields (0.21–0.49) for azaborahexahelicenes **46a**,**c** and more modest ones (~0.07) for the octa- and decahelicenes **46b**,**d**. The introduction of one additional boron atom on **46c** strongly increased the emission efficiency compared to **46a**, but at the same time strongly decreased the configuration stability (enantiomerization barrier $\Delta G^{\neq}$ of 27.5 kcal mol^{-1} at 78 °C, in ethanol) due to the presence of two azaborapentacycles. From the UV-vis spectra, the longer the helicene, the stronger were the absorption coefficients and the more red-shifted the absorption wavelengths. Similarly, the ECD spectra were more red-shifted and more intense for azaboraoctahelicene **46b** and azaboradecahelicene **46d** as compared to azaborahexahelicenes **46a**,**c**. Note that, except for **46c**, the overall ECD signature appeared typical of helicene derivatives and that the (*P*)-enantiomers display positive optical rotation values. Regarding the CPL responses, g_{lum} values were found negative for (*P*)-**46a**-**c** and positive for (*P*)-**46d** (see Table 4.6). As mentioned above, the sign of CPL greatly varies with the substituents grafted onto the helicenic core and generally follows the sign of the lower energy ECD-active band. The absolute values of g_{lum} (between 7×10^{-4} and 10^{-3}) for **46a**-**d** are typical of enantiopure organic helicenes.

Enantiopure azabora[5]helicenes **47–49** were also prepared; they displayed different charge transfer characters and fluorescence quantum yields ranging from 0.13 to 0.30 in toluene, governed by the electron-donor substitution (*p*-MeO-phenyl, *p*-Me_2N-phenyl) at the helicene [43]. The dimethylamino-substituted derivative emitted at the most red-shifted wavelength and showed the highest Stokes shift in toluene. These helicenes also showed CPL activity with dissymmetry factors g_{lum} between 2.5×10^{-4} and 3.5×10^{-3}. Their ECD spectra and optical rotation values of **47–49** were very different from azaborahelicenes **46a–d**, and it was shown that the sign of the ECD band corresponding to the first transition and the CPL spectrum depended on the electron-donor substitution.

Table 4.6 Photophysical data of borahelicenes

Compound	λ_{Abs}^{max} [a] (nm)	λ_{Em} (nm)	Φ_F (%)	Solvent (CPL)	10^3 g_{abs}	10^3 g_{lum}	Ref.
(*P*)-**46a**	398	404	21	CH_2Cl_2	~−1.9[b]	−0.9	[42]
(*P*)-**46b**	429	435	6.9	CH_2Cl_2	~−2.7[b]	−0.7	[42]
(*P*)-**46c**	391	427	49	CH_2Cl_2	~−0.8[b]	−2.3	[42]
(*P*)-**46d**	440	471	7.4	CH_2Cl_2	~+2.6[b]	+1	[42]
(*P*)-**47**	414	495	29/toluene	$CHCl_3$	−0.7	−0.25	[43]
(*P*)-**48**	420	502	30/toluene	$CHCl_3$	+1.1	+0.95	[43]
(*P*)-**49**	433	586	13/toluene	$CHCl_3$	+2	+3.5	[43]
(*P*,*P*)-**50**	411	436	65/CH_2Cl_2 (26)[b]	CH_2Cl_2	~−1.1[c]	−1.7	[44]

[a]Lowest-energy absorption band
[b]Fluorescence quantum yield measured in the solid state
[c]Taken from [12]

Oxabora[6]helicene **50** was prepared in 2016 by Hatakeyama and coworkers and revealed deep and almost pure blue fluorescence with Commission Internationale de l′Eclairage coordinates of (0.15, 0.08) [44]. Its enantiomers showed CPL high fluorescence quantum yields of 0.65 at 436 nm activity with g_{lum} of 1.7 × 10^{-3}. Achiral structural analogues of **50** have proven efficient B-containing PAH dopants in organic OLEDs and in field-effect transistors [45]. These compounds are indeed known to display good carrier mobilities. Note also that such BN and BO aromatic compounds display increasing interest in the domain of thermally activated delayed fluorescence (TADF) [46].

4.6 CPL-Active Silahelicenes

Silylated π-conjugated molecules also display strong blue emission. In 2013, Nozaki and coworkers reported the synthesis of enantiopure sila[7]helicene **51**, bearing a silole as the central cycle (Fig. 4.17) [47]. The UV-vis absorption spectrum of (*rac*)-**51** showed longest absorption at 412 nm, which is much longer than pristine phenanthrene (293 nm) and dibenzosilole (286 nm), due to extended delocalization of the π-electrons over the molecule. The absorption edge of (*rac*)-**51** at 431 nm is similar to that of λ^5-phospha[7]helicene (432 nm) and red-shifted compared to the related aza- and oxa-[7]helicenes (425 nm for aza[7]helicene and 409 nm for oxa[7]helicene). Upon excitation at 320 nm, compound (*rac*)-**51** exhibited a strong blue fluorescence with λ_{max} at 450 nm and good quantum yields in solution and

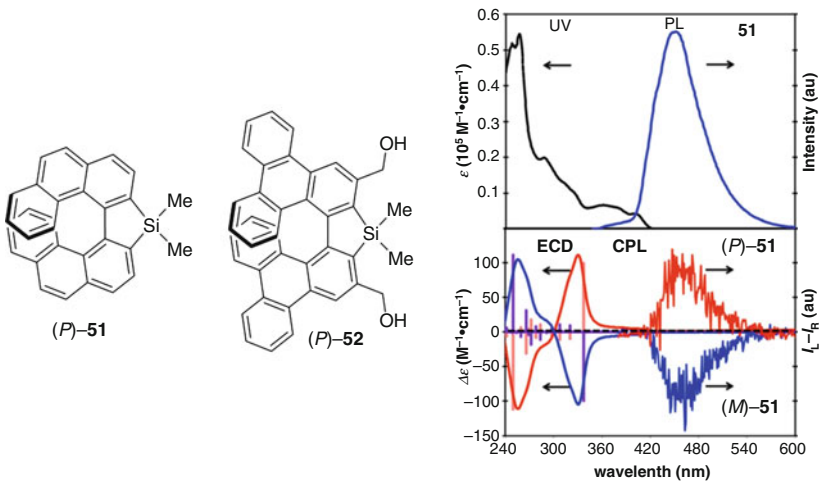

Fig. 4.17 Chemical structures of silahelicenes (*P*)-**51** and (*P*)-**52**. UV-vis/fluorescence spectra and ECD/CPL spectra of sila[7]helicene **51** in CH_2Cl_2. Blue lines in ECD and CPL spectra: (*M*)-isomer. Red lines: (*P*)-isomer. The blue and red bars show the calculated ECD spectra. Reproduced with permission [47]. Copyright 2013, American Chemical Society

Table 4.7 Photophysical data of silahelicenes

Compound	$\lambda_{Abs}{}^{max\ a}$ (nm)	λ_{Em} (nm)	Φ_F (%)	Solvent (CPL)	10^3 g_{abs}	10^3 g_{lum}	Ref.
(*P*)-**51**	412	450	23/CH_2Cl_2 (26)[b]	CH_2Cl_2	~1.4[c]	−3.5	[47]
(*P*)-**52**	400	482	6.9	$CHCl_3$	~4.2[c]	+16	[48]

[a]Lowest-energy absorption band
[b]Fluorescence quantum yield measured in the solid state
[c]Taken from [12]

in the solid state (see Fig. 4.17 and Table 4.7). The CPL spectra of enantiopure sila[7]helicene (*P*)- and (*M*)-**32**, which are mirror image of positive and negative sign, respectively; dissymmetry factors of 3.5×10^{-4} at 470 nm were measured. The authors concluded that the g_{lum} derives mainly from the helical biphenanthryl moiety, while the heterole moiety plays essential roles in the luminescent properties. In 2015, Tanaka et al. prepared enantioenriched 1,1′-bis-triphenylene-based sila[7] helicenes (*P*)-**52** with 91% *ee* [48]. Compared to sila[7]helicene **51**, **52** displayed red-shifted absorption and fluorescence responses explained by the presence of fused 1,1′-bistriphenylenes resulting in more extended π-conjugation. Probably for the same reason, enantiopure **52** show high g_{lum} values, i.e., 1.6×10^{-2}, which is uncommonly high for an organic helicene. These values appear larger than that for the 3,3-biphenanthrene-based sila[7]helicene **51** ($g_{lum} = -0.0035$ at 470 nm) but smaller than that for the 1,1-bitriphenylene based carbo[7]helicene **61** ($g_{lum} = -0.030$ at 428 nm for the (*M*)-(−) enantiomer; see Sect. 4.8.3) [49].

4.7 CPL-Active Phosphahelicenes

It is now well recognized that phosphorus-containing π-conjugated small molecules, oligomers, polymers, and supramolecular assemblies are important classes of heteroatomic molecular materials for many applications in optoelectronics including OLEDs [50]. P-containing building blocks can indeed lead to materials with unique properties (emission, charge transport, coordination, (anti)aromaticity, etc.). So far, most phosphorus derivatives having helical chirality have displayed polyaromatic (or heteroaromatic) helical scaffolds with pendant phosphorus functions (phosphites, trivalent phosphines and phosphine oxides, helicene-phospholes derivatives) but a few classes of P-containing heterohelicenes have appeared in the literature in the last years. Although several phospholes and helicenes are known to exhibit efficient fluorescence properties, the only example of CPL-active phosphane-containing helicenes has been reported recently [51]. Compounds **53a** and **53b** are benzooxophosphole derivatives that display a carbo[6] helicene unit that is *meta*-fused with one terminal oxophosphole ring containing a pendant phenyl ring at position 5 (Fig. 4.18). In both systems a *l*-menthyl group at the P atom is directed toward the inner groove of the helix (*endo* isomer).

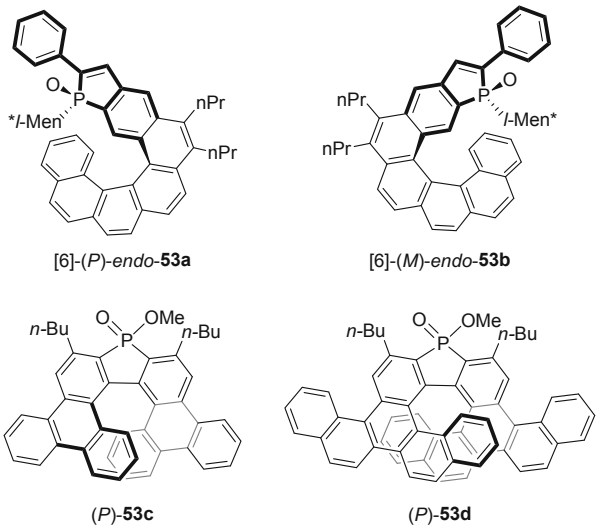

Fig. 4.18 CPL-active phosphahelicenes

Table 4.8 Photophysical data of phosphahelicenes

Compound	λ_{Abs} $^{max\ a}$ (nm)	λ_{Em} (nm)	Φ_F (%)	Solvent	10^3 g_{abs}	10^3 g_{lum}	Ref.
(*P*)-(+)-**53a**	436	449	10	CH_2Cl_2	–	+0.8	[51]
(*M*)-(−)-**53b**	438	455	7	CH_2Cl_2	–	−0.7	[51]
(+)-**53c**[b]	388	487	22	$CHCl_3$	–	+0.81	[52]
(+)-**53d**[b]	315	502	8.5	$CHCl_3$	–	+0.48	[52]

[a]Lowest energy UV-vis band
[b]Absolute configuration not determined

These epimeric compounds can be considered as pseudo-enantiomers since they demonstrate reverse stereochemistry of the helix (*P*/*M*) and of the P atom (R_P/S_P) but unchanged stereochemistry of the chiral *l*-menthyl group. The epimeric helicenes [6]-(*P*)-*endo*-**53a** and [6]-(*M*)-*endo*-**53b** displayed almost identical UV-vis spectra, blue fluorescence with moderate quantum yield (0.07–0.10), and mirror-image ECD spectra. Similarly, they exhibited mirror-image CPL spectra with luminescence anisotropy factor $g_{lum} = +8 \times 10^{-4}$ and -7×10^{-4} at 452 nm (excitation at 404–416 nm) for (*P*)-**53a** and (*M*)-**53b**, respectively (Table 4.8). Note that the other phosphahelicenes tested underwent photodegradation under the conditions of the CPL measurement.

In 2018, Tanaka and coworkers reported the enantioselective synthesis of [7]- and [9]phosphahelicenes **53c** and **53d** (Fig. 4.18) by [2+2+2] cycloaddition. These heterohelicenes displayed modest quantum yields (0.22 and 0.085) and g_{lum} values ($+8.1 \times 10^{-4}$ and $+3.8 \times 10^{-4}$) [52].

4.8 CPL-Active Carbohelicenic Derivatives

4.8.1 Pentahelicenic Structures

In 2018, Mori and coworkers reported a combined experimental and theoretical study to elucidate the ECD and CPL behaviors of parent pentahelicene (*P*)-**23** and of D_3-symmetric triple pentahelicene (*P*,*P*,*P*)-**54** [53]. They showed that the pentahelicene unit exhibits absorption and luminescence, with dissymmetry factors g_{abs} and g_{lum} that are intrinsically larger than those of higher homologues. Thus, (*P*)-**23** emitted strong CPL with g_{lum} of -2.7×10^{-3} at low temperature (see Table 4.9 and Fig. 4.19), which is about a half value of the g_{abs}. Due to its photolabile nature, **23** is not suitable to be incorporated in chiroptical materials. However, such undesirable reactivities can be excluded by merging three pentahelicenic units into **54**, for which the g_{lum} and g_{abs} factors were found to be as high as -1.3×10^{-3} and -1.8×10^{-3}, respectively, for the (*P*) enantiomer, corresponding to a high g_{lum}/g_{abs} ratio of 0.72, indicating moderate excited-state relaxation. Theoretical calculations provided further insights into the improved chiroptical responses at the main band (^1B_b transition) in the triple pentahelicene **23**, which was ascribed to its symmetric nature.

In 2017, Lu and coworkers prepared enantiopure tetrahydrocarbo[5]helicenic derivatives (Fig. 4.20) with high configurational stability, thanks to the presence of phenyl groups placed in the inner groove of the helix [54]. These compounds displayed strong blue fluorescence with quantum yield of up to 0.59. Compounds (*P*)-(+)-**55a-e**,**56** and (*M*)-(−)-**55a-e**,**56** also exhibited mirror-imaged ECD and

Table 4.9 Photophysical data of pentahelicenic derivatives

Compound	$\lambda_{Abs}{}^{max\ a}$ (nm)	λ_{Em} (nm)	Φ_F (%)	Solvent (CPL)	$10^3\ g_{abs}$	$10^3\ g_{lum}$	Ref.
(*P*)-(+)-**23**	398	406	5.7	CH_2Cl_2	−7.6	−2.7	[53]
(*M*)-(−)-**54**	460	483	1.8	CH_2Cl_2	−1.8	−1.3	[53]
(*P*)-(+)-**55a**	347	440	48	THF	2.63	5.63	[54]
(P)-(+)-**55b**	349	442	59	THF	3.55	3.66	[54]
(*P*)-(+)-**55c**	344	439	40	THF	4.34	6.32	[54]
(*P*)-(+)-**55d**	344	438	41	THF	3.82	6.41	[54]
(*P*)-(+)-**55e**	345	440	42	THF	3.21	4.58	[54]
(*P*)-(+)-**56**	338	465	3	THF	7.87	28.2	[54]
(*P*)-(−)-**57a**	305	424	32.6	CH_2Cl_2	−0.47	−0.25	[55]
(*P*)-(−)-**57b**	310	425	41.0	CH_2Cl_2	−0.50	−0.28	[55]
(*P*)-(−)-**57c**	301	425	39.1	CH_2Cl_2	−0.83	−0.41	[55]
(*P*)-(+)-**57d**	330	455	18.7	CH_2Cl_2	−0.328	−4.52	[55]

[a]Lowest-energy UV-vis band

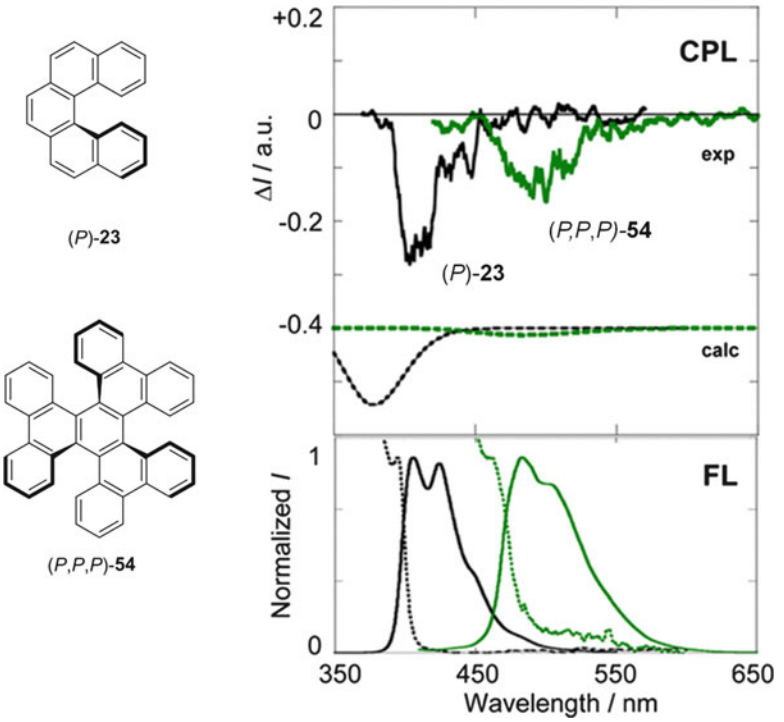

Fig. 4.19 Chemical structures, fluorescence, and CPL activity of pentahelicenic (*P*)-**23** and of D_3-symmetric triple pentahelicene (*P*,*P*,*P*)-**54**. Adapted with permission [53]. Copyright 2018, American Chemical Society

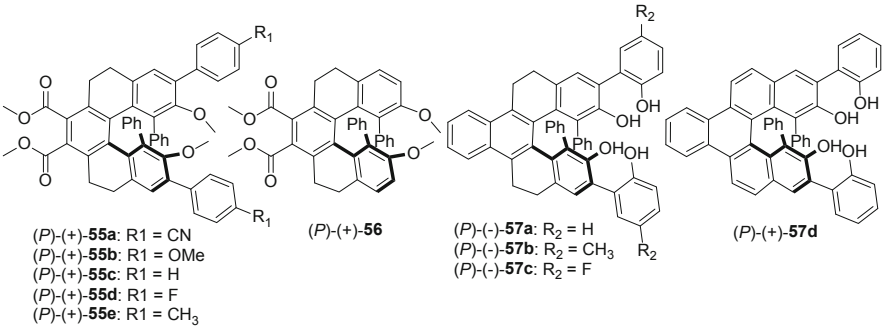

Fig. 4.20 Enantioenriched tetrahydrocarbo[5]helicenic derivatives prepared by Chen et al

CPL spectra in THF. Due to similar helical backbones, all systems showed similar Cotton effects with strong negative Cotton effects at ~290 nm and positive ones at 315–320 nm for the (*P*)-(+)-**55a-e**,**56** enantiomers. The g_{abs} values were found within the range of $+2.63 \times 10^{-3}$ to $+4.77 \times 10^{-3}$ for the (*P*) enantiomers

and -3.40×10^{-3} to -2.73×10^{-3} for the (*M*) enantiomers, respectively. These compounds also showed intense CPL signals, matching with the region of emission spectra and corresponding ECD signals at the longest wavelength (305–400 nm). The pure enantiomers all exhibited relatively high g_{lum} with values between $+3.66 \times 10^{-3}$ and $+ 6.41 \times 10^{-3}$ for the (*P*) configurations and -3.40×10^{-3} to -6.59×10^{-3} for the (*M*) configurations (Table 4.9) thus showing that chirality existed in both the ground and excited states and could be attributed to their rigid helical structures. Interestingly, absorption dissymmetry factors (g_{abs}) of (*P*)-(+)-**56** and (*M*)-(−)-**56** were found stronger ($+7.9 \times 10^{-3}$ and -7.7×10^{-3}, respectively), as well as the emission dissymmetry factors (g_{lum}) as large as 2.8×10^{-2} and -3.1×10^{-2} at 466 nm, respectively, considerably higher than values reported for other CPL-active single organic molecules. Similar tetrahydropentahelicenic structures, i.e., (*P*)-(−)-**57a-c** and (*M*)-(+)-**57a-c**, were prepared in 2018 by Chen et al. [55]. They exhibited mirror-image ECD and CPL spectra in dichloromethane, with g_{abs} of -4.7×10^{-4} to -8.3×10^{-4} for the (*P*) configuration, and $+4.9 \times 10^{-4}$ to $+8.7 \times 10^{-4}$ for the (*M*) configuration (Table 4.10 and [55]). As for fully conjugated derivative pentahelicene (*P*)-(+) and (M)-(−)-**57d**, they display g_{abs} values of similar magnitude ($+3.28 \times 10^{-4}$ and -3.57×10^{-4}, respectively). Furthermore, the enantiomers of **57a–c** showed CPL signals with g_{lum} values between -2.5×10^{-4} and -4.1×10^{-4} for the (*P*) enantiomers and $+2.6 \times 10^{-4}$ and $+4.2 \times 10^{-4}$ for the (*M*) ones. (*P*)-(+) and (*M*)-(−)-**57d** in dichloromethane exhibited stronger CPL activity, with g_{lum} values of -4.52×10^{-3} and $+4.43 \times 10^{-3}$, respectively. In 2018, Chen et al. also reported the one-pot oxidative aromatization and dearomatization (OADA) reactions of similar tetrahydro[5]helicene diols, with DDQ as the oxidant, which provided a new method for the synthesis of novel CPL-active chiral π-extended diones [58].

Table 4.10 Photophysical data of carbon-based helicenes

Compound	$\lambda_{Abs}{}^{max\ a}$ (nm)	λ_{Em} (nm)	Φ (%)	Solvent (CPL)	10^3 g_{abs}	10^3 g_{lum}	Ref.
(*P*)-**58a**	582	610	39	CH_2Cl_2	+0.15	+0.1	[56]
(*P*)-**58b**	582	610	41	CH_2Cl_2	+0.9	+0.6	[56]
(*P*,*P*)**58c**	622	650	35	CH_2Cl_2	+1.3	+0.9	[56]
(*P*)-(+)-**59a**	326	442	14	$CHCl_3$	−0.56	~0	[57]
(*P*)-(+)-**59b**	327	452	29	$CHCl_3$	−3.1	~0	[57]
(*P*,*P*)-(+)-**59c**	291	464	11	$CHCl_3$	−0.68	−2.7	[57]
(*P*,*P*)-(+)-**59d**	292	466	7.6	$CHCl_3$	−4.5	−1.5	[57]
(*P*)-**10**	410	413	14	$CHCl_3$	−1.2[b]	−0.9	[23]
(*P*)-**11**	410	416	5	$CHCl_3$	−2.5[b]	−0.02[b]	[20]
(*P*,*P*)-**60**	471	494	1.8	CH_2Cl_2	−2.6	−2.5	[23]
(*P*,*P*)-**61**	430	434	4.1	CH_2Cl_2	−2.8	−2.1	[23]

[a]Lowest energy UV-vis band
[b]Taken from [12]

4.8.2 CPL-Active Hexahelicenic Structures

Hexahelicenic derivatives are prototypic helicenes exhibiting CPL activity. In 2018, our group showed that grafting diketopyrrolopyrrole (dpp) dyes onto a carbo[6]helicene structure through ethynyl bridges (see **58a–c** in Fig. 4.21) leads to exciton coupling circular dichroism in the red region arising from the achiral - red-absorbing DPP units in the helical environment [56]. Furthermore, red to near-infrared circularly CPL was obtained. Indeed, the association of enantiopure [6] helicene and dpp units provided helical π-conjugated molecules with strong ECD signal in the visible region (~600 nm), intense red and near-infrared fluorescence ($\phi_F \sim 0.4$), and CPL activity up to 650 nm with g_{lum} found to increase from 1×10^{-4} to 6×10^{-4} then 9×10^{-4} with the increase of exciton coupling (i.e., through the series **58a** → **58b** → **58c**). The g_{abs} values were also found to follow the same increasing trend with the increasing exciton coupling. These results highlighted the synergy between the chiral hexahelicene structure and the organic dye. Thus, decorating carbohelicenes with dyes constitutes an appealing strategy of chemical engineering of a π-helical platform to further improve the chiroptical responses.

In 2018, Tanaka and coworkers reported the enantioselective synthesis of fully benzenoid single (**59a**,**b**) and double (**59c**,**d**) carbo[6]helicenes via efficient gold-catalyzed intramolecular hydroarylation (Fig. 4.22) [57]. Similar to the single (**12–14**) and double azahelicenes (**15–16**) described in Sect. 4.2.3, the double carbo[6]helicenes **59c**,**d** exhibited relatively large CPL activities (up to 2.7×10^{-3}, see Table 4.10), as compared to the single carbo[6]helicenes **59a**,**b** whose CPL was below the limit of the apparatus.

In 2018, X-shaped and S-shaped pristine double hexahelicenes (**60** and **61**, Fig. 4.23) were prepared and used as representative molecular models, and a theory-guided, symmetry-based protocol was developed [23]. Compound **60** and **61** exhibited a strong increase in intensity of ECD and CPL. The enhanced chiroptical responses were theoretically assigned to the electric (μ_e) and magnetic (μ_m) transition dipole moments of component hexahelicenes aligned in the correct symmetry. Indeed, **60** and **61**, constructed by merging two hexahelicenes in D_2 and C_2 symmetry, respectively, showed absorption dissymmetry factors per benzene unit (g_{abs}/n) for the ^1B_b band that are larger by a factor of up to 1.5 than that of parent **10**. This enhancement was well rationalized by μ_e and μ_m and their relative angle (θ) evaluated theoretically. In the double helicenes, μ_e and μ_m were parallel-aligned ($\theta = 0$) to maximize the orientation factor (cos θ) up to unity, which was mere 0.24 (cos 76°) in **10**, while $|\mu_e|$ and $|\mu_m|$ were comparable or only slightly improved. Similarly, the luminescence dissymmetry factor per benzene unit (g_{lum}/n) was up to 1.7-fold larger for the double helicenes than for **10**, for which the increased $|\mu_e|$ and θ are responsible. The enhanced g_{abs}/n and g_{lum}/n values for double helicenes mean that merging two helicenes is 50–70% more resource efficient than simply assembling them, in favor of the molecular, rather than supramolecular strategy for constructing advanced chiroptical devices.

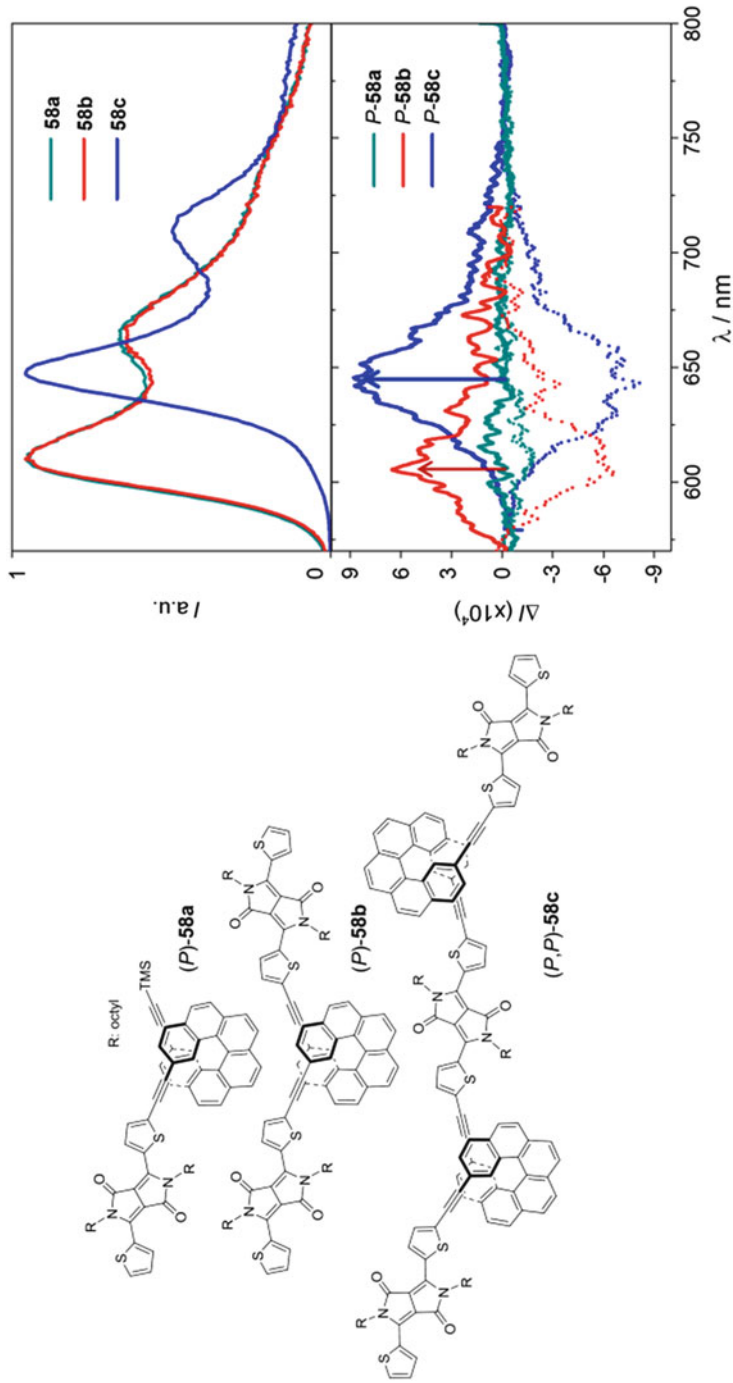

Fig. 4.21 Chemical structures, fluorescence, and CPL spectra in CH_2Cl_2 of hexahelicene-dpp derivatives (*P*)-**58a–c**. Adapted with permission [56]. Copyright 2018, Royal Society of Chemistry

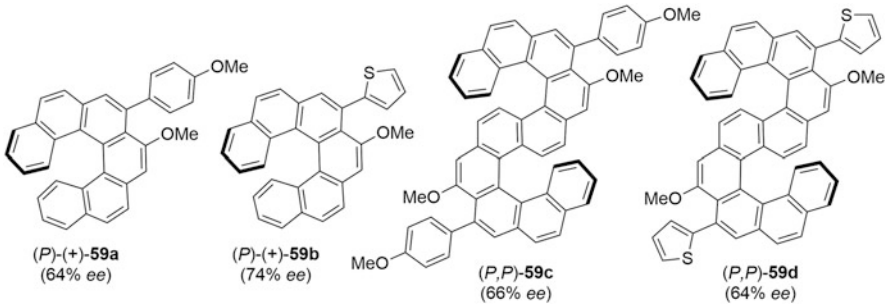

Fig. 4.22 Chemical structures of enantioenriched single carbo[6]helicenes **59a**,**b** and S-shaped double carbo[6]helicenes **59c**,**d** [57]

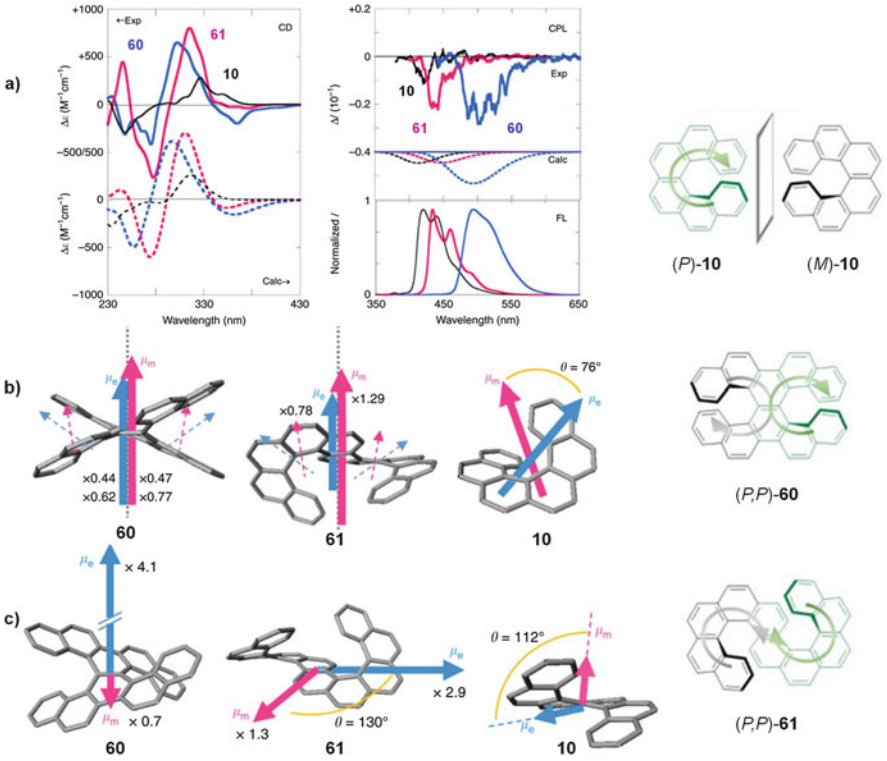

Fig. 4.23 (**a**) Experimental and calculated ECD and CPL responses of **10**, **60,** and **61** ((*P*) enantiomers). (**b**) Transition dipole moments in the ground state. Schematic representations of electric (μ_e, blue) and magnetic (μ_m, red) transition dipole moments of the ^1B_b band for X-shaped and S-shaped double hexahelicenes **60** and **61**, with the magnitudes relative to parent helicene **10**, calculated at the RI-CC2/def2-TZVPP level. Dashed arrows in double helicenes indicate the transition dipole moments of component helicene units. (**c**) Transition dipole moments in the excited state. Schematic representations of the electric (μ_e, blue) and magnetic (μ_m, red) transition dipole moments of the ^1L_b band of **60** and **61** in the excited states, with the magnitudes relative to those for parent helicene **10**, calculated at the RI-CC2/def2-TZVPP level. Adapted with permission [23]. Copyright 2018, Nature Publishers

4.8.3 CPL-Active Heptahelicenic Structures

In 2012, Tanaka et al. reported the preparation of helically chiral 1,1′-bitriphenylenes displaying a central fluorenyl cycle. These compounds correspond to heptahelicenic structures and exhibit among the strongest CPL activity [59]. Indeed, compounds **62** and **63** (Fig. 4.24) obtained with high enantiomeric excesses (93% and 91% *ee,* respectively) exhibited mirror-imaged CPL spectra with particularly high fluorescence dissymmetry factors ($g_{lum} = -0.030$ at 428 nm for (*M*)-(−)-**62** and $g_{lum} = -0.032$ at 449 nm for (*M*)-(−)-**63** in chloroform, Table 4.11), which are comparable to phthalhydrazide-functionalized [7]helicene-like molecule **34** ($g_{lum} = -0.035$ at 476 nm for the assembly state and −0.021 for the molecularly dispersed state) and significantly larger than those for helically chiral molecules reported to date. However, the g_{lum} values are found very high compared to the g_{abs} values, which are around 2.5–2.9 × 10^{-3}, i.e., one order of magnitude lower. This is clearly seen in the ECD shape, which displays the typically large bands of (*P*)-helicenes (a large positive band at ~320 nm, and two large negative bands at ~260 and 285 nm, Fig. 4.25) but small bands between 340 and 400 nm which correspond to the lowest energy transitions. Later on in 2016, Nozaki and coworkers reported the synthesis and photophysical properties of enantiopure [7]helicene-like fluorenyl systems **64a**,**b** [60]. These compounds showed similar absorption spectra with the longest absorption maximum at ~400 nm slightly blue-shifted compared to that of carbo[7]helicene, while they are significantly red-shifted compared to those of fluorene and phenanthrene. Indeed, the π-conjugation is well extended over the whole molecule despite their helically twisted structures. In addition, the longest absorption maximum is slightly red-shifted compared to that of compound **62** despite the fact that **62** possesses triphenylene units [57]. This phenomenon may be attributed to a smaller twist of compounds **64** than compound **62**, resulting in more effective π-conjugation along the helical structure. [7]Helicene-like compounds **64a**,**b** exhibited an emission maximum at around 420 nm with a very small Stokes shift and high fluorescence quantum yields (up to 40%) among the highest reported helicenes at that time and slightly higher than those of [7]helicene-like compounds [59]. This makes helicenes incorporating a fluorene unit very appealing for highly emissive chiral molecular materials. ECD spectra of **64a**,**b** enantiomers display a similar shape as for **62** and

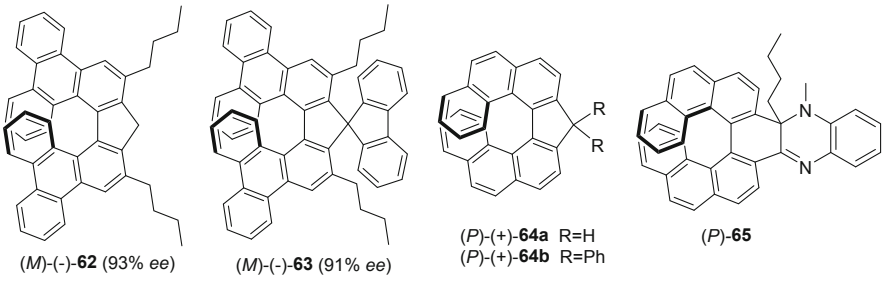

(*M*)-(-)-**62** (93% *ee*) (*M*)-(-)-**63** (91% *ee*) (*P*)-(+)-**64a** R=H (*P*)-(+)-**64b** R=Ph (*P*)-**65**

Fig. 4.24 Chemical structures of CPL-active heptahelicenic derivatives

Table 4.11 Photophysical data of heptahelicenic derivatives

Compound	λ_{Abs} $^{max\ a}$ (nm)	λ_{Em} (nm)	Φ (%)	Solvent (CPL)	10^3 g_{abs}	10^3 g_{lum}	Ref.
(*M*)-(−)-**62**	388	428	32	$CHCl_3$	−2.5[b]	−30	[59]
(*M*)-(−)-**63**	400	449	29.6	$CHCl_3$	−2.9[b]	−32	[59]
(*P*)-(+)-**64a**	400	417	39	CH_2Cl_2	1.3[b]	3	[60]
(*P*)-(+)-**64b**	408	421	40	CH_2Cl_2	–	2.5	[60]
(*P*)-(+)-**65**	435	550	25	THF	−1.3	−4	[61]

[a]Lowest energy UV-vis band
[b]Taken from [12]

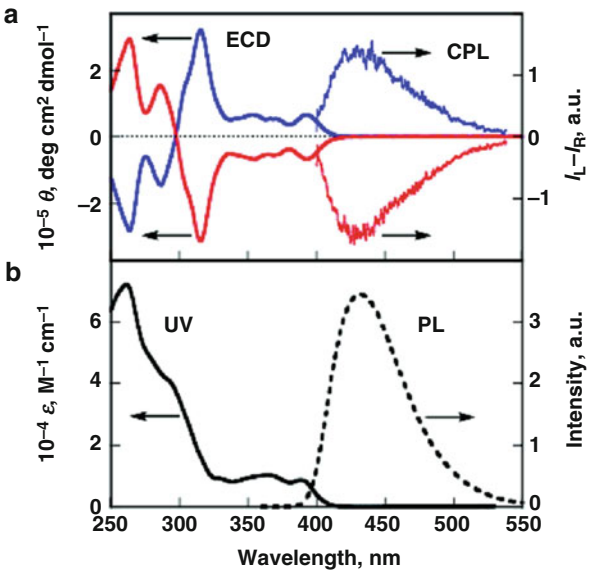

Fig. 4.25 (**a**) ECD/CPL spectra of heptahelicenic fluorene **63** in CH_2Cl_2. Blue lines in ECD and CPL spectra: (*P*)-isomer. Red lines: (*M*)-isomer and (**b**) UV-vis/fluorescence spectra. Reproduced with permission [59]. Copyright 2012, American Chemical Society

63 but their CPL activities were smaller, with dissymmetry factors of 3.0×10^{-3} and 2.5×10^{-3}, respectively. These values are comparable to that of silole-fused compound **51** (vide supra). In 2015, Hasobe and coworkers reported a highly yellow fluorescent [7]carbohelicene fused by asymmetric 1,2-dialkyl-substituted quinoxaline (**65**) [61]. It displayed a fluorescence quantum yield of 0.25 at 550 nm emission wavelength which is more than 10 times larger than that of the pristine heptahelicene ($\Phi_F = 0.02$). Such a large enhancement of fluorescence in **65** also provided good CPL activity, with g_{lum} values of $\pm 4.0 \times 10^{-3}$. A negative CPL signal for the (*P*)-(+) isomer, i.e., an S-type one (vide supra and [20, 22]), corresponding to the small negative ECD signal at 435 nm with a g_{abs} of -1.3×10^{-3}. Note also that this compound was successfully used as an emitter in OLEDs but the authors did not report any CPL emission of the OLED.

4.9 CPL-Active Transition Metal Complexes of Helicenes

4.9.1 Cycloplatinated Helicenes

Coordination chemistry offers a simple way to tune the optical and electronic properties of the π-ligands since both the coordination sphere geometry and the nature of the metal-ligand interaction can be readily modified by varying the metal center. This will produce a great impact on the properties of the molecule [62]. Recent studies have demonstrated many potential applications of N-containing helicenes in coordination chemistry and in materials science [63]. Indeed, their transition metal complexes may show interesting properties in harvesting (visible) light and re-emitting it at a wavelength that depends on the metallic ion used, thus allowing the development of light-emitting devices, chemosensors, photovoltaic dye-sensitized devices, etc. In 2010, our group prepared the first class of organometallic helicenes incorporating a metallic ion, i.e., Pt, within their helical backbone, named platinahelicenes [64, 65]. Enantiopure platina[6]helicene **66a**, platina[8]helicene **66b**, bisplatina[6]helicene **66c**, and bisplatina[10]helicene **66d** (Fig. 4.26), displayed absorption spectra that were strongly red-shifted compared to the starting ligands, with longer absorption wavelengths above 450 nm. Furthermore, platinahelicenes **66a-d** are efficient deep-red phosphors, with emission maxima between 630 and 700 nm, quantum yields around 0.05–0.10 in deoxygenated solution at room temperature and luminescence lifetimes of 10–20 μs. Interestingly, platinahelicenes **66a–c** displayed circularly polarized phosphorescence with dissymmetry factors as high as 10^{-2}, which is one order of magnitude bigger than for most of organic helicenes. These g_{lum} values appeared positive for the (*P*) enantiomers and negative for the (*M*), which was not always the case in azaborahelicenes analogues **46a–d** [45]. Note that bis-platina[10]helicene **66d** also exhibited red

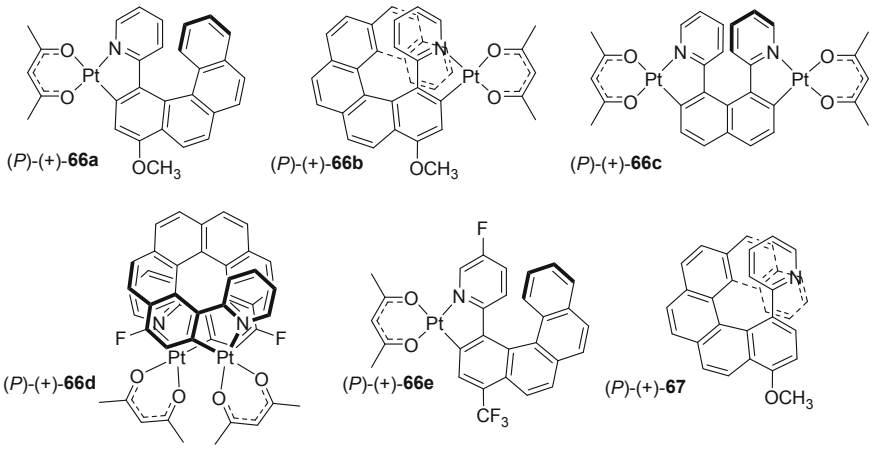

Fig. 4.26 Chemical structures of platinahelicenes **66a–e** and of precursor **67**

phosphorescence at room temperature, but no CPL activity was detected. This can be explained by the weakly chiral environment around the two Pt centers and the high sensitivity to oxygen. Note also that the precursor 1-(2-pyridyl)-hexahelicene **67** displayed fluorescence emission and CPL activity (see Table 4.12). Recently, polyfluorinated platina[6]helicene **66e** was prepared by Zheng et al. [66] It displayed similar molecular behavior as **66a–c**, namely red phosphorescence, and CPL activity with a g_{lum} of -3.7×10^{-3} in dichloromethane solution for the (*P*)-(+) enantiomer. The same compound displayed a g_{lum} of -4.1×10^{-3} when incorporated in a DCzppy film (DCzppy: 2,6-bis(3-(9H-carbazol-9-yl)phenyl)pyridine). Interestingly, compounds **66a** and **66e** were used as chiral dopants in OLED devices to conceive efficient circularly polarized OLEDs (CP-OLEDs; see Sect. 4.10).

4.9.2 Coordination of Helicene-Bipyridine Ligands

Our group also prepared complexes bearing a helicene-bipyridine-type ligand. Bipyridine ligands are classical N^N chelate ligands but can also act as C^N ones toward different transition metal ions such as platinum. In 2015, we reported the preparation of enantiopure helical cycloplatinated complexes (*P*)- and (*M*)-**69** from a [6]helicene-bipyridine-type ligand, namely, 3-(2-pyridyl)-4-aza[6]helicene ((*P*)- and (*M*)-**68** in Fig. 4.27) [67]. Due to the presence of an additional N atom in organometallic species (*P*)- and (*M*)-**69**, the acid-base triggering of UV-vis, ECD,

Table 4.12 Photophysical data of platinahelicenes and helicene-bipy rhenium complexes

Compound	$\lambda_{Abs}^{max\ a}$ (nm)	λ_{Em} (nm)	Φ (%)	Solvent (CPL)	10^3 g_{abs}	10^3 g_{lum}	Ref.
(*P*)-(+)-**66a**	452	644	10	CH_2Cl_2	~3.5[b]	+13	[65]
(*P*)-(+)-**67**	422	430	–	CH_2Cl_2	~7.3[b]	+0.8	[65]
(*P*)-(+)-**66b**	467	648	5.6	CH_2Cl_2	~12[b]	+0.5	[65]
(*P*)-(+)-**66c**	471	633	13	CH_2Cl_2	~3.2[b]	+0.4	[65]
(*P*)-(+)-**66d**	479	639	6.6	CH_2Cl_2	–	~0	[65]
(*P*)-(+)-**66e**	463	612	27	CH_2Cl_2	–	−3.7 (−4.1)[c]	[66]
(*M*)-(−)-**68**	417	421	8.4	CH_2Cl_2	~−4.1[b]	−3.2	[67]
(*M*)-(−)-**68**.2H$^+$	418	590	8.2	CH_2Cl_2	~−5.3[b]	−2.9	[67]
(*M*)-(−)-**69**	430	547	0.38	CH_2Cl_2	~−5.2	−1.1	[67]
(*M*)-(−)-**69**.H$^+$	450	555	2.7	CH_2Cl_2	~−10	−2	[67]
((*M*,C_{Re})-**70a**[2]	445	673	0.16	CH_2Cl_2	~−2	−3	[68]
(*M*)-**71a**[1,2]	444	598	6	CH_2Cl_2	~−0.4	−1.5	[68]

[a]Lowest-energy UV-vis band
[b]Taken from [12]
[c]Fluorescence quantum yield measured in a DCzppy film

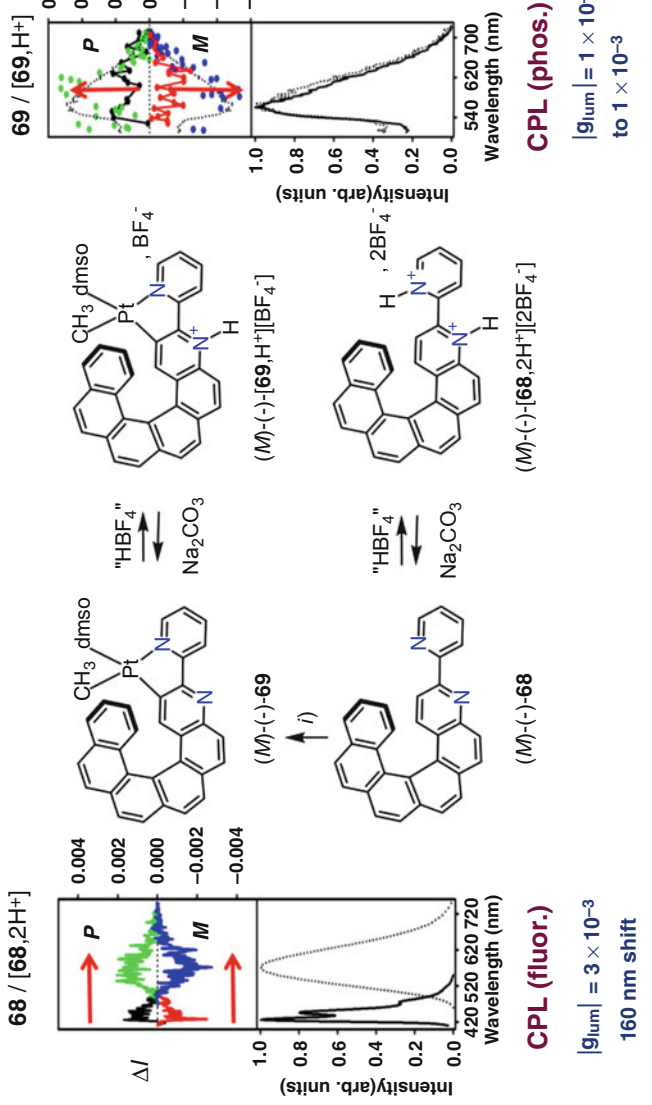

Fig. 4.27 Synthesis of cycloplatinated helicene (*M*)-**69** from (*M*)-**68** and reversible protonation and deprotonation process of organic and organometallic systems, observed by emission and CPL spectroscopies. (*i*) $Pt(dmso)_2(CH_3)_2$, acetone, 50 °C, 5 h, 90%. Variation of emission and CPL responses upon protonation [67]

phosphorescence, and CPL were achieved, thus yielding the first acid-based CPL switch (see the increase of g_{lum} upon protonation in Fig. 4.27). Furthermore, we showed that organic helicene ligand (*P*)- and (*M*)-**68** was also an efficient chiroptical switch since, after double protonation, it displayed a strong bathochromic shift in emission wavelength while keeping strong CPL fluorescence signal ($g_{lum} = \pm 2 \times 10^{-3}$ in CH_2Cl_2). TDDFT calculations showed that, upon protonation, the HOMO-to-LUMO transition changed from a π–π∗-type to a charge transfer-type transition.

Rhenium(I)-chloro-tricarbonyl complexes bearing a bipy ligand are known to display efficient luminescence, usually a ^{3}CT emission from an excited state based on the bis-imine ligand. In this context, organic helicene-bipy ligand (*P*)- and (*M*)-**68** was used as N^N chelate to prepare enantioenriched CPL-active helicene-bipyridine-rhenium complexes **70** (Fig. 4.28) [68]. Starting from (*M*)-**68** ligand, two diastereomeric complexes, i.e., (*M*,A_{Re})-**70a^1** and (*P*,C_{Re})-**70a^2**, were formed, since the Re(I) atom is also a stereogenic center. These stereoisomers were separated by regular silica gel column chromatography and their chiroptical and emissive properties were studied. They revealed strong ECD spectra in CH_2Cl_2 (whose intensity depends on the rhenium stereochemistry; see Fig. 4.28), accompanied by substantial phosphorescence and CPL activity. Indeed (*M*,A_{Re})-**70a^1** and (*M*,C_{Re})-**70a^2** displayed phosphorescence emission (λ_{max}^{phos} = 673–680 nm, ϕ = 0.13–0.16%, τ = 27–33 ns) and good g_{lum} values ((*M*,C_{Re})-**70a^2**: $g_{lum} \sim -3 \times 10^{-3}$ around 670 nm). Upon reaction with AgOTf and 2,6-dimethylphenyl isocyanide in the presence of NH_4PF_6, (*M*,C_{Re}) and (*P*,A_{Re})-**71a^2** were transformed to cationic complexes (*P*)- and (*M*)-**71a^{1,2}**, respectively (see Fig. 4.28). The latter displayed stronger phosphorescence (λ_{max}^{phos} = 598 nm, ϕ = 6%, τ = 79 μs) and still good CPL activity ($g_{lum} \sim \pm 1.5 \times 10^{-3}$). However, the stereochemical information at the Re (I) center was lost (epimerization to 50:50 mixture). Nevertheless, the ECD spectrum of (*P*)-**71a^{1,2}** displayed an additional positive ECD-active band around 450 nm as compared to (*P*,C_{Re})-**114a^1** and (*P*,A_{Re})-**70a^2**. According to TDDFT calculations, this band does not involve the Re center but corresponds to the HOMO-to-LUMO transition with strong intra-ligand charge transfer from the π-helicene to the bipy moiety [68]. We have thus shown that the incorporation of a rhenium atom within an extended helical π-conjugated bipyridine system can impact the chiroptical and photophysical properties of the resulting neutral or cationic complexes, leading to the first rhenium-based circularly polarized phosphors.

4.9.3 Coordination Chemistry of Bis-Helicene-Terpyridine and Bis-Helicene-Bipy Ligands

In 2016, our group also prepared the bis-helical terpyridine (terpy) ligand **72** which acted as a chiroptical switch upon reversible coordination-decoordination to zinc(II). The strong conformational changes induced led to a multi-responsive chiroptical

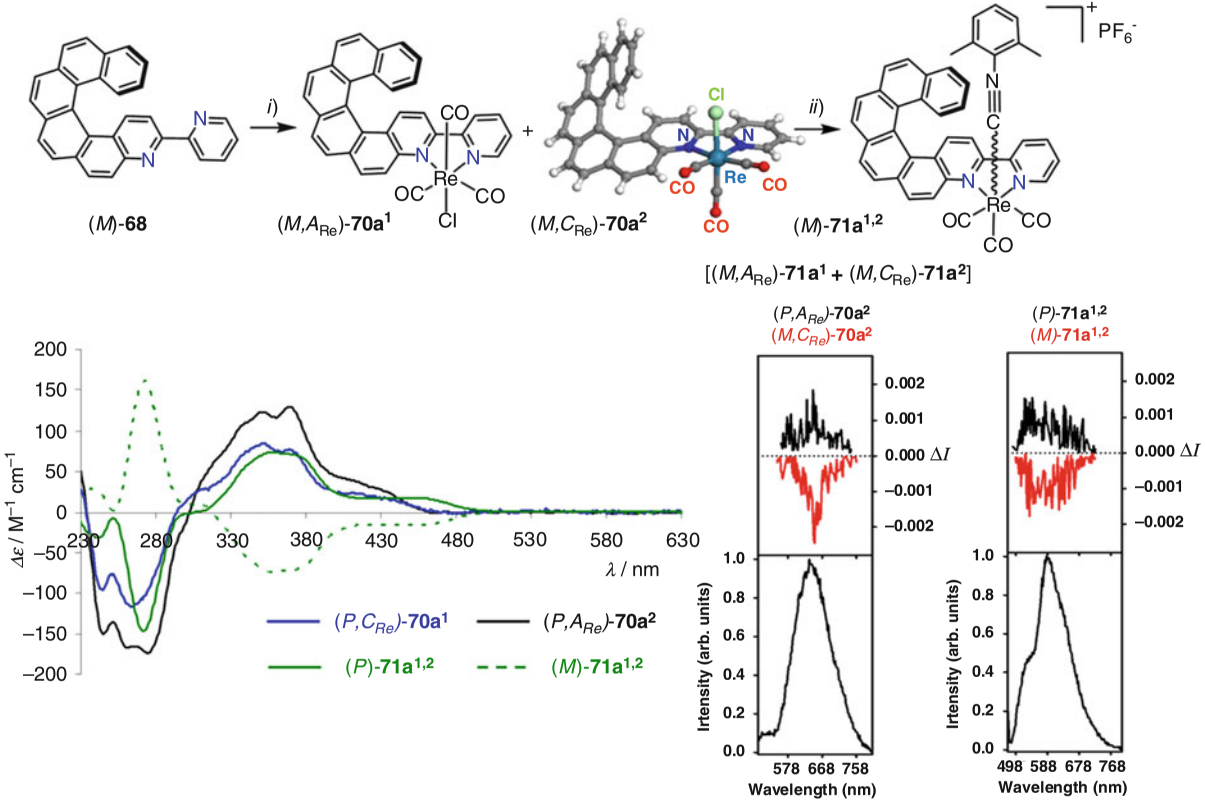

Fig. 4.28 Synthesis of enantioenriched rhenium complexes (M,A_{Re})-**70a**^{1}, (M,C_{Re})-**70a**^{2}, and (M)-**71a**^{1,2} (mixture of two diastereomers). (*i*) $Re(CO)_5Cl$, toluene, reflux; (*ii*) AgOTf, EtOH/THF, then 2,6-dimethylphenyl isocyanide, THF, NH_4PF_6. X-ray crystallographic structure of **70a**^{2}. ECD spectra of (P,C_{Re})-**70a**^{1}, (P,A_{Re})-**70a**^{2} and $(M)/(P)$-**71a**^{1,2} isomers (CH_2Cl_2). Phosphorescence and CPL spectra of (P,C_{Re})-**70a**^{1}, (P,A_{Re})-**70a**^{2} and $(M)/(P)$-**71a**^{1,2} isomers in CH_2Cl_2 [68]

switch (Fig. 4.29) [69]. The interconversion between the ligand and zinc-complexed states was analyzed via first-principles calculations, which highlighted the change from π-π∗ transitions in the organic ligand to charge transfer transitions in the Zn complex. Overall, this system behaved as a chiroptical switch offering multi-output readout (UV-vis, ECD, luminescence, and CPL). Furthermore, the switching process triggered conformational changes and molecular motion around the Zn center, from a clear *trans* (W-shape) conformation in the free ligand to a *cis* (U-shape) one in the Zn-complex **73** (Fig. 4.29, Table 4.13). Recently, we have prepared a novel enantiopure bis-helicenic 2,2′-bipyridine system ligand, **74** [70]. Thanks to the bipyridine unit, the coordination to **75** with Zn^{II} and protonation processes to **74.**$2H^+$ were studied revealing efficient tuning of photophysical (UV-vis and emission) and chiroptical properties (ECD and CPL) of the system (Fig. 4.29, Table 4.13). The coordination-decoordination and protonation/deprotonation processes appeared reversible thus constituting novel chiroptical switches.

4.9.4 CPL-Active Iridium Complexes from Helicene-NHC Ligands

In the last two decades, octahedral cyclometalated iridium(III) complexes have attracted attention due to their appealing properties as phosphors in high-efficiency organic light-emitting devices (OLEDs) [71]. In 2017, the first fused π-helical NHC system was prepared and examined through its diastereoisomerically pure cyclometalated complexes *mer*-(*P*,Λ_{Ir})-**77a**$^{\mathbf{1}}$ and *mer*-(*P*,Δ_{Ir})-**77a**$^{\mathbf{2}}$ from pentahelical imidazolium **76** (Fig. 4.30) [49]. These chiral organometallic species displayed light-green phosphorescence with (*i*) circular polarization that depends on both the -helical-NHC (*P*)/(*M*) stereochemistry and the iridium (*Δ*)/(*Λ*) one (Fig. 4.30 and Table 4.14) and (*ii*) unusually long lifetimes (up to 250 μs as compared to 530 ns for model *mer*-**78**). The unprecedented features of **77a**$^{\mathbf{1,2}}$ can be attributed to extended π-conjugation within helical carbenic ligand. A similar cycloiridiated complex, namely, *mer*-(Δ_{Ir}/Λ_{Ir})-**79**, bearing a NHC N-substituted with a carbo[4]helicene unit was recently obtained and also displayed long-lived mirror-image circularly polarized phosphorescence (Table 4.14) [72].

4.10 Applications in Optoelectronics

There is an obvious interest to develop the use of helicenes and helicenoids as chiral molecular materials in chiral OLEDs, in chiral sensors, in chiral bioimaging agents, chiroptical switching activity [73, 74] applications that directly take benefit from circularly polarized emission. For instance, there is a strong potential of CP

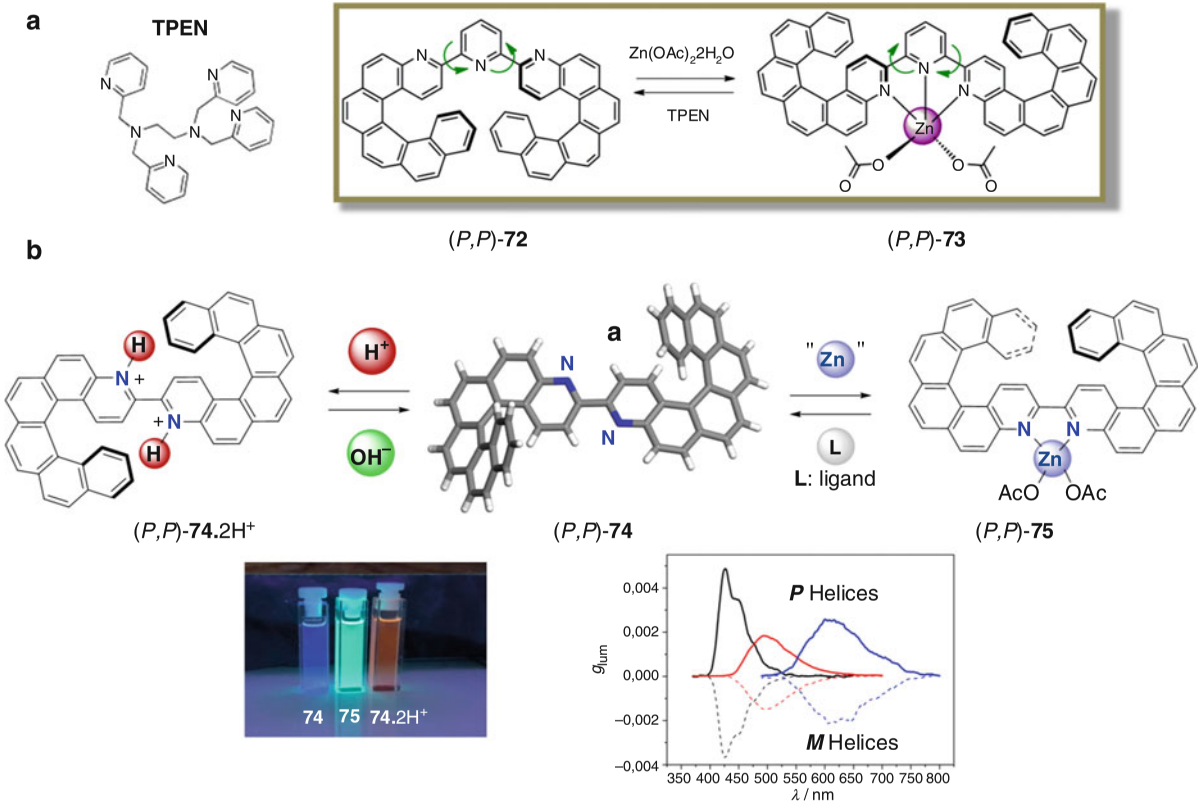

Fig. 4.29 (**a**) Reversible Zn(II) complexation-decomplexation process of (*P*,*P*)-**72** to (*P*,*P*)-**73** using $Zn(OAc)_2$ and TPEN as the chemical stimuli [69]. (**b**) Reversible Zn(II) complexation-decomplexation process of (*P*,*P*)-**74** to (*P*,*P*)-**75** using $Zn(OAc)_2$ and TPEN as the chemical stimuli and acid-base triggered switch between (*P*,*P*)-**74** and (*P*,*P*)-**74**.$2H^+$. Emission colors and CPL activity of **72** (black), **75** (red) and **74**.$2H^+$ (blue). Plain lines are for the (*P*) helicenes and dotted lines for the (*M*) ones. Adapted with permission [70]. Copyright 2019, American Chemical Society

Table 4.13 Photophysical data of helicene-bipy and terpy ligands together with heir Zn and proton complexes

Compound	$\lambda_{Abs}{}^{max\ a}$ (nm)	λ_{Em} (nm)	Φ (%)	Solvent (CPL)	10^3 g_{abs}	10^3 g_{lum}	Ref.
(*P*,*P*)-(+)-**72**	416	421	8.4	CH_2Cl_2	~6.5[b]	+8.6	[69]
(*P*,*P*)-(+)-**73**	430	480	19	CH_2Cl_2	~4.3[b]	+1.2	[69]
(*P*,*P*)-(+)-**74**	420	421	22	CH_2Cl_2	–	+4.8	[70]
(*P*,*P*)-(+)-**75**	453	520	44	CH_2Cl_2	–	+1.8	[70]
(*P*,*P*)-(+)-**74**.$2H^+$	507	600	28	CH_2Cl_2	–	+2.5	[70]

[a]Lowest-energy UV-vis band
[b]Taken from 12

light technologies in the development of OLEDs in which the electroluminescence is directly circularly polarized thus giving CP-OLEDs. Indeed, antiglare filters commonly used for OLED displays exploit the physics of CP light to eliminate glare from external light sources (e.g., the sunlight). Unfortunately, this technology removes approximately 50% of the non-polarized light emitted from the OLED pixels. If the non-polarized OLEDs are replaced with CP-OLEDs (with a comparable device performance), an improved amount of CP light component of the correct handedness would pass through the antiglare filter with less loss, thus increasing the energy efficiency of the display in proportion to the increasing dissymmetry of the light. In addition, the use of CP-OLED will enable to simplify the architecture of the device by avoiding the use of extra filter components, which will directly impact the overall cost of the device.

In 2013, Fuchter and coworkers, reported the use of 1-aza[6]helicene **9** as a chiral dopant in light-emitting polymer, i.e., poly[9,9-dioctylfluorene-*co*-benzothiadiazole] **80** (Fig. 4.31a) [21]. It was found that blends consisting of a small amount (7%) of enantiopure 1-aza[6]helicene dopant gave a strong CP-photoluminescence response of the **80** films. Increasing the 1-aza[6]helicene blending ratio resulted in improvements of the g_{PL} factor, up to a significantly high value of 0.5 for the 53% helicene blend (while the starting azahelicene displayed only modest g_{lum} ~10^{-4} to 10^{-3}). To explain this behavior, the authors suggested the formation of a chiroptical co-crystalline phase. The authors were then able to fabricate a single-layer polymer LED (PLED) device emitting circularly polarized light from the **80** blends containing 7% of either (−)-1-aza[6]helicene or (+)-1-aza[6]helicene with a dissymmetry factor of electroluminescence (g_{EL}) factor as high as 0.2. In 2016, Fuchter and Campbell succeeded in preparing a single layer CP-phosphorescent OLEDs (CP-PHOLEDs), using **66a** as a chiral emissive dopant; these PHOLEDs displayed strong circularly polarized electrophosphorescence (CPEL), with g_{EL} reaching −0.38 and + 0.22 at 615 nm for (−)- and (+)-**66a**, respectively (see Fig. 4.31b) [75]. Although not yet clearly demonstrated, the increase of g_{EL} as compared to the molecular g_{lum} value (10^{-2}) may be explained by a supramolecular organization of **66a** in the solid state. Recently, by decorating the pyridyl-helicene ligands with $–CF_3$ and –F groups [66], the platinahelicene enantiomers **66e** featured good configurational stability as well as high sublimation

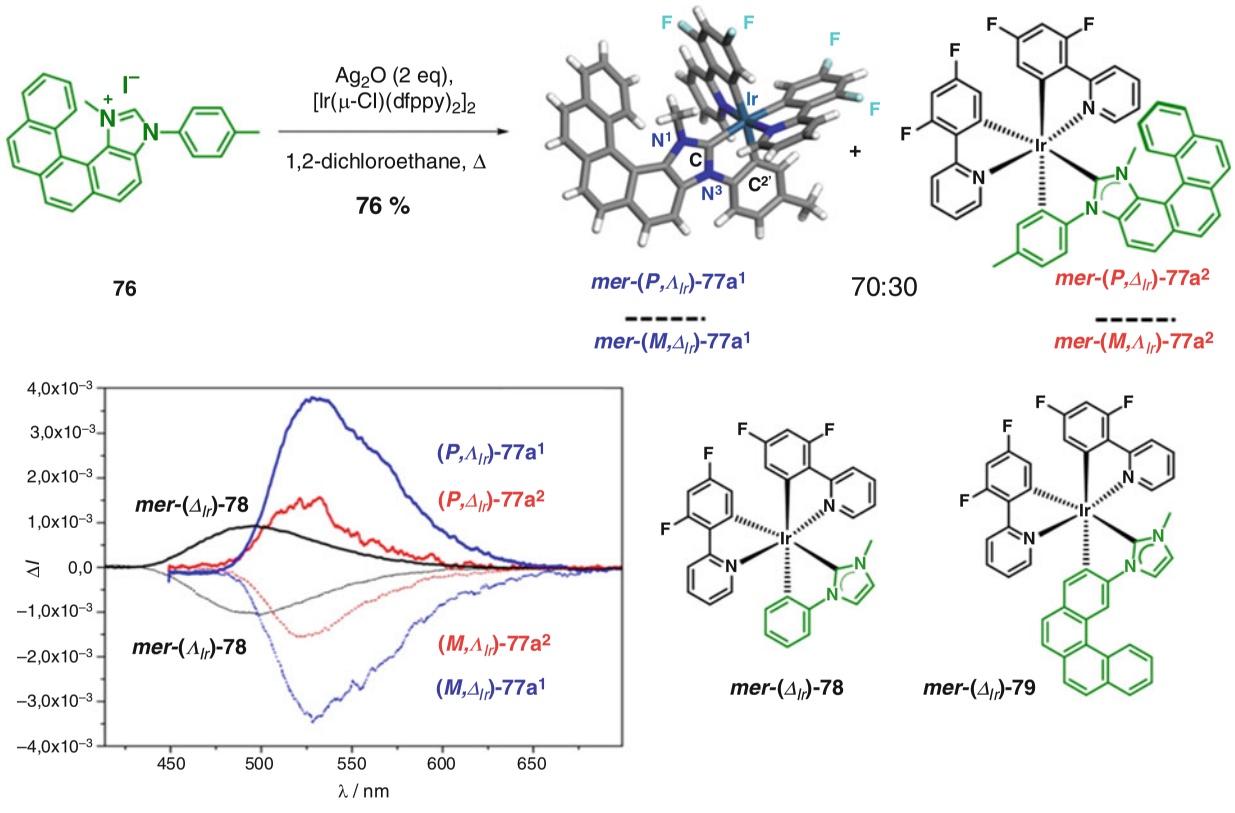

Fig. 4.30 Preparation of cycloiridiated complexes **77**[1,2]. Chemical structures and CPL spectra of iridium(III) complexes (P,Λ_{Ir})-**77a**[1]/(M,Δ_{Ir})-**77a**[1], (P,Δ_{Ir})-**77a**[2]/(M,Λ_{Ir})-**77a**[2], and (Δ_{Ir})-**78**/(Λ_{Ir})-**78**. Chemical structure of (Δ_{Ir})-**79**. X-ray structure of stereoisomer(P,Λ_{Ir})-**77a**[1]. All complexes have the *mer* geometry [49, 72]

Table 4.14 Photophysical data of helicene-NHC iridium complexes

Compound	λ_{Abs} $^{max\ a}$ (nm)	λ_{Em} (nm)	Φ (%)	Solvent (CPL)	10^3 g_{lum}	Ref.
(P,Δ_{Ir})-(+)-**77a**[1]	402	525	9	CH_2Cl_2	+3.7	[49]
(P,Λ_{Ir})-(+)-**77a**[2]	403	526	13	CH_2Cl_2	+1.5	[49]
(Δ_{Ir})-(+)-**78**	390	498	29	CH_2Cl_2	+0.9	[49]
(Δ_{Ir})-(+)-**79**	394	510	5	CH_2Cl_2	+3.1	[72]

[a]Lowest-energy UV-vis band

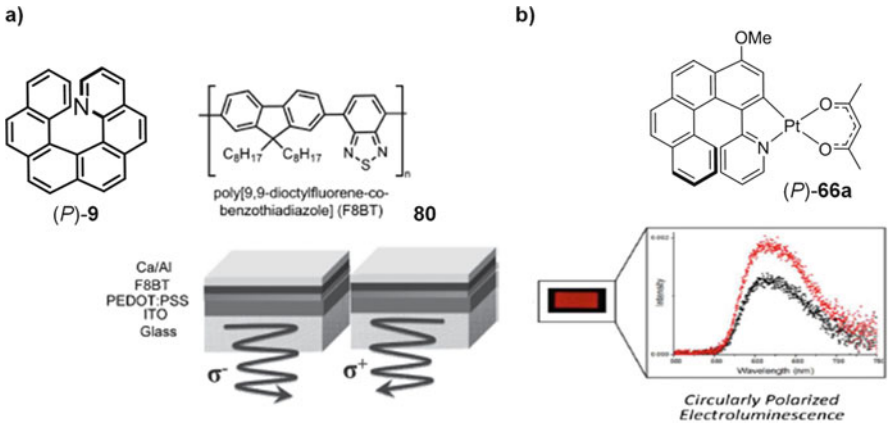

Fig. 4.31 (**a**) CP-PLED based on blends between enantiopure **9** and **80**. Adapted with permission 19 Copyright 2013, Wiley. (**b**) CP-PHOLED based on pure enantiopure cycloplatinahelicene **66a**. Adapted with permission [75]. Copyright 2016, American Chemical Society

yield (>90%) and clear circularly polarized phosphorescence, with dissymmetry factors ($|g_{PL}|$) of approximately 3.7×10^{-3} in solution and about 4.1×10^{-3} in doped films. The CP-PHOLEDs with two enantiomers as emitters exhibited symmetric CPEL signals with $|g_{EL}|$ of $(1.1–1.6) \times 10^{-3}$ and good device performances, achieving a maximum brightness of 11,590 cd m^{-2}, a maximum external quantum efficiency up to 18.81%, which are the highest values among the reported devices based on chiral phosphorescent Pt^{II} complexes. To suppress the effect of reverse CPEL signal from the cathode reflection, the further implementation of semi-transparent aluminum/silver cathode successfully boosted up the $|g_{EL}|$ by over three times to 5.1×10^{-3}.

4.11 Conclusion

Since the first examples of helicenes displaying circularly polarized luminescence described in the literature [13, 37], there has been a growing interest in CPL-active helicenes and helicenoids, and the number of reported examples is growing

very fast. This is concomitant to the development of helicenes chemistry and the creation of structural diversity of helical structures, either fully carbonated or containing main-group elements, and to the development of CPL instrumentations and CPL technology. However, a much higher degree of circular polarization is still highly desirable for applications, for example, in chiroptical devices. For this purpose, future work will be probably dedicated to the development of supramolecular architectures, sophisticated homogeneous/heterogeneous mixtures, aggregation induced emission (AIE) materials, or chiral TADF systems, to obtain good CPL properties together with overall good quantum yield of photoluminescence. In these domains, there is still plenty of room for fundamental discoveries and for further applications. Finally, although not detailed in the present chapter, theoretical calculations of CPL activity may be of great help to anticipate highly efficient CPL-active systems. In this context, CPL-active helicenes are good models for testing and improving theoretical tools.

References

1. Dekkers HPJM (2000) Circularly polarized luminescence: a probe for chirality in the excited state. In: Berova N, Nakanishi K, Woody RW (eds) Circular dichroism: principles and applications. Wiley-VCH, New York, pp 185–215
2. Riehl JP, Muller G (2012) Circularly polarized luminescence spectroscopy and emission-detected circular dichroism. In: Berova N, Polavarapu PL, Nakanishi K, Woody RW (eds) Comprehensive chiroptical spectroscopy, vol 1. Wiley, Hoboken
3. Maeda H, Bando Y (2013) Recent progress in research on stimuli responsive circularly polarized luminescence based on π-conjugated molecules. Pure Appl Chem 85:1967–1978
4. Kumar J, Nakashima T, Kawai T (2015) Circularly polarized luminescence in chiral molecules and supramolecular assemblies. J Phys Chem Lett 6:3445–3452
5. Sánchez-Carnerero EM, Agarrabeitia AR, Moreno F, Maroto BL, Muller G, Ortiz MJ, de la Moya S (2015) Circularly polarized luminescence from simple organic molecules. Chem Eur J 21:13488–13500
6. Chen N, Yan B (2018) Recent theoretical and experimental progress in molecules circularly polarized luminescence of small organic molecules. Molecules 23:3376
7. Shen Y, Chen C-F (2012) Helicenes: synthesis and applications. Chem Rev 112:1463–1535
8. Chen C-F, Shen Y (2017) Helicene chemistry: from synthesis to applications. Springer, Berlin
9. Gingras M (2012) One hundred years of Helicene chemistry. Part 3: applications and properties of carbohelicenes. Chem Soc Rev 42:1051–1095
10. Newman MS, Lednicer D (1956) The synthesis and resolution of hexahelicene. J Am Chem Soc 78:4765–4770
11. Zinna F, Di Bari L (2015) Lanthanide circularly polarized luminescence: bases and applications. Chirality 27:1–13
12. Tanaka H, Inoue Y, Mori T (2018) Circularly polarized luminescence and circular dichroisms in small organic molecules: correlation between excitation and emission dissymmetry factors. ChemPhotoChem 2:386–402
13. Field JE, Muller G, Riehl JP, Venkataraman D (2003) Circularly polarized luminescence from bridged triarylamine helicenes. J Am Chem Soc 125:11808–11809
14. Longhi G, Castiglioni E, Villani C, Sabia R, Menichetti S, Viglianisi C, Devlin F, Abbate S (2016) Chiroptical properties of the ground and excited states of two thia-bridged triarylamine heterohelicenes. J Photochem Photobiol A 331:138–145

15. Nishimura H, Tanaka K, Morisaki Y, Chujo Y, Wakamiya A, Murata Y (2017) Oxygen-bridged diphenylnaphthylamine as a scaffold for full-color circularly polarized luminescent materials. J Org Chem 82:5242–5249
16. Liu Y, Cerezo J, Mazzeo G, Lin N, Zhao X, Longhi G, Abbate S, Santoro F (2016) Vibronic coupling explains the different shape of electronic circular dichroism and of circularly polarized luminescence spectra of hexahelicenes. J Chem Theory Comput 12:2799–2819
17. Nakamura K, Furumi S, Takeuchi M, Shibuya T, Tanaka K (2014) Enantioselective synthesis and enhanced circularly polarized luminescence of S-shaped double azahelicenes. J Am Chem Soc 136:5555–5558
18. Tanaka M, Shibata Y, Nakamura K, Teraoka K, Uekusa H, Nakazono K, Takata T, Tanaka K (2016) Gold-catalyzed enantioselective synthesis, crystal structure, and photophysical/chiroptical properties of aza[10]helicenes. Chem Eur J 22:9537–9541
19. Otani T, Tsuyuki A, Iwachi T, Someya S, Tateno K, Kawai H, Saito T, Kanyiva KS, Shibata T (2017) Facile two-step synthesis of 1,10-phenanthroline-derived polyaza[7]helicenes with high fluorescence and CPL efficiency. Angew Chem Int Ed 56:3906–3910
20. Abbate S, Longhi G, Lebon F, Castiglioni E, Superchi S, Pisani L, Fontana F, Torricelli F, Caronna T, Villani C, Sabia R, Tommasini M, Lucotti A, Mendola D, Mele A, Lightner DA (2014) Helical sense-responsive and substituent-sensitive features in vibrational and electronic circular dichroism, in circularly polarized luminescence, and in Raman spectra of some simple optically active hexahelicenes. J Phys Chem C 118:1682–1695
21. Yang Y, da Costa RC, Smilgies D-M, Campbell AJ, Fuchter MJ (2013) Induction of circularly polarized electroluminescence from an achiral light-emitting polymer via a chiral small-molecule dopant. Adv Mater 25:2624–2628
22. Nakai Y, Mori T, Sato K, Inoue Y (2013) Theoretical and experimental studies of circular dichroism of mono and diazonia[6]helicenes. J Phys Chem A 117:5082–5092
23. Tanaka H, Ikenosako M, Kato Y, Fujiki M, Inoue Y, Mori T (2018) Symmetry-based rational design for boosting chiroptical responses. Commun Chem 1:38
24. Goto K, Yamaguchi R, Hiroto S, Ueno H, Kawai T, Shinokubo H (2012) Intermolecular oxidative annulation of 2-aminoanthracenes to diazaacenes and aza[7]helicenes. Angew Chem Int Ed 51:10333–10336
25. Ushiyama A, Hiroto S, Yuasa J, Kawai T, Shinokubo H (2017) Synthesis of a figure-eight azahelicene dimer with high emission and CPL properties. Org Chem Front 4:664–667
26. Sakai H, Kubota T, Yuasa J, Araki Y, Sakanoue T, Takenobu T, Wada T, Kawai T, Hasobe T (2016) Synthetic control of photophysical process and circularly polarized luminescence of [5]carbohelicene derivatives substituted by maleimide units. J Phys Chem C 120:7860–7869
27. Sakai H, Kubota T, Yuasa J, Araki Y, Sakanoue T, Takenobu T, Wada T, Kawai T, Hasobe T (2016) Protonation-induced red-coloured circularly polarized luminescence of [5]carbohelicene fused by benzimidazole. Org Biomol Chem 14:6738–6743
28. Li M, Lu H-Y, Zhang C, Shi L, Tang Z, Chen C-F (2016) Helical aromatic imide based enantiomers with full color circularly polarized luminescence. Chem Commun 52:9921–9924
29. Delgado IH, Pascal S, Wallabregue A, Duwald R, Besnard C, Guenee L, Nancoz C, Vauthey E, Tovar RC, Lunkley JL, Muller G, Lacour J (2016) Functionalized cationic [4]helicenes with unique tuning of absorption, fluorescence and chiroptical properties up to the far-red range. Chem Sci 7:4685–4693
30. Pascal S, Besnard C, Zinna F, Di Bari L, Le Guennic B, Jacquemin D, Lacour J (2016) Zwitterionic [4]helicene: a water-soluble and reversible PH-triggered ECD/CPL chiroptical switch in the UV and red spectral regions. Org Biomol Chem 14:4590–4594
31. Bosson J, Labrador GM, Pascal S, Miannay FA, Yushchenko O, Li H, Bouffier L, Sojic N, Tovar RC, Muller G, Jacquemin D, Laurent AD, Le Guennic B, Vauthey E, Lacour J (2016) Physicochemical and electronic properties of cationic [6]helicenes: from chemical and electrochemical stabilities to far-red (polarized) luminescence. Chem Eur J 22:18394–18403
32. Kaseyama T, Furumi S, Zhang X, Tanaka K, Takeuchi M (2011) Hierarchical assembly of a phthalhydrazide-functionalized helicene. Angew Chem Int Ed 50:3684–3687

33. Yamano R, Hara J, Murayama K, Sugiyama H, Teraoka K, Uekusa H, Kawauchi S, Shibata Y, Tanaka K (2017) Rh-mediated enantioselective synthesis, crystal structures, and photophysical/chiroptical properties of phenanthrenol-based[9]helicene-like molecules. Org Lett 19:42–45
34. Matsuno T, Koyama Y, Hiroto S, Kumar J, Kawai T, Shinokubo H (2015) Isolation of a 1, 4-diketone intermediate in oxidative dimerization of 2-hydroxyanthracene and its conversion to oxahelicene. Chem Commun 51:4607–4610
35. Gupta R, Cabreros TA, Muller G, Bedekar AV (2018) Enantiomerically pure 5,13-dicyano-9-oxa[7]helicene: synthesis and study. Eur J Org Chem 2018:5397–5405
36. Sundar MS, Talele HR, Mande HM, Bedekar AV, Tovar RC, Muller G (2014) Synthesis of enantiomerically pure helicene like bis-oxazines from atropisomeric 7,7′-dihydroxy BINOL: preliminary measurements of the circularly polarized luminescence. Tetrahedron Lett 55:1760–1764
37. Phillips KES, Katz TJ, Jockusch S, Lovinger AJ, Turro NJ (2001) Synthesis and properties of an aggregating heterocyclic helicene. J Am Chem Soc 123:11899–11907
38. Riehl JP, Richardson FS (1986) Circularly polarized luminescence spectroscopy. Chem Rev 86:1–16
39. Yamamoto Y, Sakai H, Yuasa J, Araki Y, Wada T, Sakanoue T, Takenobu T, Kawai T, Hasobe T (2016) Controlled excited-state dynamics and enhanced fluorescence property of tetrasulfone[9]helicene by a simple synthetic process. J Phys Chem C 120:7421–7427
40. Yamamoto Y, Sakai H, Yuasa J, Araki Y, Wada T, Sakanoue T, Takenobu T, Kawai T, Hasobe T (2016) Synthetic control of the excited-state dynamics and circularly polarized luminescence of fluorescent "push–pull" tetrathia[9]helicenes. Chem Eur J 22:4263–4273
41. Biet T, Cauchy T, Sun Q, Ding J, Hauser A, Oulevey P, Bürgi T, Jacquemin D, Vanthuyne N, Crassous J, Avarvari N (2017) Triplet state CPL active helicene–dithiolene platinum bipyridine complexes. Chem Commun 53:9210–9213
42. Shen C, Srebro-Hooper M, Jean M, Vanthuyne N, Toupet L, Williams JAG, Torres AR, Riives AJ, Muller G, Autschbach J, Crassous J (2017) Synthesis and chiroptical properties of hexa-, octa-, and decaazaborahelicenes: influence of helicene size and of the number of boron atoms. Chem Eur J 23:407–418
43. Dominguez Z, Lopez-Rodriguez R, Alvarez E, Abbate S, Longhi G, Pischel U, Ros A (2018) Azabora[5]helicene charge-transfer dyes show efficient and spectrally variable circularly polarized luminescence. Chem Eur J 24:12660–12668
44. Katayama T, Nakatsuka S, Hirai H, Yasuda N, Kumar J, Kawai T, Hatakeyama T (2016) Two-step synthesis of boron-fused double helicenes. J Am Chem Soc 138:5210–5213
45. Miyamoto F, Nakatsuka S, Yamada K, Nakayama K, Hatakeyama T (2015) Synthesis of boron-doped polycyclic aromatic hydrocarbons by tandem intramolecular electrophilic arene borylation. Org Lett 17:6158–6161
46. Hatakeyama T, Shiren K, Nakajima K, Nomura S, Nakatsuka S, Kinoshita K, Ni J, Ono Y, Ikuta T (2016) Ultrapure blue thermally activated delayed fluorescence molecules: efficient HOMO-LUMO separation by the multiple resonance effect. Adv Mater 28:2777–2781
47. Oyama H, Nakano K, Harada T, Kuroda R, Naito M, Nobusawa K, Nozaki K (2013) Facile synthetic route to highly luminescent Sila[7]helicene. Org Lett 15:2104–2107
48. Murayama K, Oike Y, Furumi S, Takeuchi M, Noguchi K, Tanaka K (2015) Enantioselective synthesis, crystal structure, and photophysical properties of a 1,1′-bitriphenylene-based sila[7]helicene. Eur J Org Chem 2015:1409–1414
49. Hellou N, Srebro-Hooper M, Favereau L, Zinna F, Caytan E, Toupet L, Dorcet V, Jean M, Vanthuyne N, Williams JAG, Di Bari L, Autschbach J, Crassous J (2017) Enantiopure cycloiridiated complexes bearing a pentahelicenic N-heterocyclic carbene and displaying long-lived circularly-polarized phosphorescence. Angew Chem Int Ed 56:8236–8239
50. Duffy MP, Delaunay W, Bouit P-A, Hissler M (2016) π-Conjugated phospholes and their incorporation into devices: components with a great deal of potential. Chem Soc Rev 45:5296–5310

51. Yavari K, Delaunay W, De Rycke N, Reynaldo T, Aillard P, Srebro-Hooper M, Chang VY, Muller G, Tondelier D, Geffroy B, Voituriez A, Marinetti A, Hissler M, Crassous J (2019) Phosphahelicenes: from chiroptical and photophysical properties to OLED applications. Chem Eur J 25:5303–5310
52. Nishigaki S, Murayama K, Shibata Y, Tanaka K (2018) Rhodium-mediated enantioselective synthesis of a benzopicene-based phospha[9]helicene: the structure–property relationship of triphenylene- and benzopicene-based carbo- and phosphahelicenes. Mater Chem Front 2:585–590
53. Tanaka H, Kato Y, Fujiki M, Inoue Y, Mori T (2018) Combined experimental and theoretical study on circular dichroism and circularly polarized luminescence of configurationally robust D_3-symmetric triple pentahelicene. J Phys Chem A 122:7378–7384
54. He D-Q, Lu H-Y, Li M, Chen C-F (2017) Intense blue circularly polarized luminescence from helical aromatic esters. Chem Commun 53:6093–6096
55. Fang L, Li M, Lin W-B, Chen C-F (2018) Enantiopure (*P*)- and (*M*)-3,14-bis(*O*-hydroxyaryl) tetrahydrobenzo[5]helicenediols and their helicene analogues: synthesis, amplified circularly polarized luminescence and catalytic activity in asymmetric hetero-Diels–Alder reactions. Tetrahedron 74:7164–7172
56. Dhbaibi K, Favereau L, Srebro-Hooper M, Jean M, Vanthuyne N, Zinna F, Jamoussi B, Di Bari L, Autschbach J, Crassous J (2018) Exciton coupling in diketopyrrolopyrrole-helicene derivatives leads to red and near-infrared circularly polarized luminescence. Chem Sci 9:735–742
57. Satoh M, Shibata Y, Tanaka K (2018) Enantioselective synthesis of fully benzenoid single and double carbohelicenes via gold-catalyzed intramolecular hydroarylation. Chem Eur J 24:5434–5438
58. Fang L, Li M, Lin W-B, Shen Y, Chen C-F (2018) One-pot oxidative aromatization and dearomatization of tetrahydro[5]helicene diols: synthesis, structure, photophysical and chiroptical properties of chiral π-extended diones. Asian J OrgChem 12:2518–2526
59. Sawada Y, Furumi S, Takai A, Takeuchi M, Noguchi K, Tanaka K (2012) Rhodium-catalyzed enantioselective synthesis, crystal structures, and photophysical properties of helically chiral 1,1-bitriphenylenes. J Am Chem Soc 134:4080–4083
60. Oyama H, Akiyama M, Nakano K, Naito M, Nobusawa K, Nozaki K (2016) Synthesis and properties of [7]helicene-like compounds fused with a fluorene unit. Org Lett 18:3654–3657
61. Sakai H, Shinto S, Kumar J, Araki Y, Sakanoue T, Takenobu T, Wada T, Kawai T, Hasobe T (2015) Highly fluorescent [7]carbohelicene fused by asymmetric 1,2-dialkyl-substituted quinoxaline for circularly polarized luminescence and electroluminescence. J Phys Chem C 119:13937–13947
62. Saleh N, Shen C, Crassous J (2014) Helicene-based transition metal complexes: synthesis, properties and applications. Chem Sci 5:3680–3694
63. Ou-Yang J-K, Crassous J (2018) Chiral multifunctional molecules based on organometallic helicenes: recent advances. Coord Chem Rev 376:533–547
64. Norel L, Rudolph M, Vanthuyne N, Williams JAG, Lescop C, Roussel C, Autschbach J, Crassous J, Réau R (2010) Metallahelicenes: easily accessible helicene derivatives with large and tunable chiroptical properties. Angew Chem Int Ed 49:99–102
65. Shen C, Anger E, Srebro M, Vanthuyne N, Deol KK, Jefferson TD, Muller G, Williams JAG, Toupet L, Roussel C, Autschbach J, Réau R, Crassous J (2014) Straightforward access to mono- and bis- cycloplatinated helicenes displaying circularly polarized phosphorescence by using crystallization resolution methods. Chem Sci 5:1915–1927
66. Yan Z-P, Luo X-F, Liu W-Q, Wu Z-G, Liang X, Liao K, Wang Y, Zheng Y-X, Zhou L, Zuo J-L, Pan Y, Zhang H (2019) Configurationally stable platinahelicene enantiomers for efficient circularly polarized phosphorescent organic light-emitting diodes. Chem Eur J 25:5672–5676
67. Saleh N, Moore B, Srebro M, Vanthuyne N, Toupet L, Williams JAG, Roussel C, Deol KK, Muller G, Autschbach J, Crassous J (2015) Acid/base-triggered switching of circularly

polarized luminescence and electronic circular dichroism in organic and organometallic helicenes. Chem Eur J 21:1673–1681
68. Saleh N, Srebro M, Reynaldo T, Vanthuyne N, Toupet L, Chang VY, Muller G, Williams JAG, Roussel C, Autschbach J, Crassous J (2015) Enantio-enriched CPL-active helicene-bipyridine-rhenium complexes. Chem Commun 51:3754–3757
69. Isla H, Srebro-Hooper M, Jean M, Vanthuyne N, Roisnel T, Lunkley JL, Muller G, Williams JAG, Autschbach J, Crassous J (2016) Conformational changes and chiroptical switching of enantiopure bis-helicenic terpyridine upon Zn^{2+} binding. Chem Commun 52:5932–5935
70. Isla H, Saleh N, Ou-Yang J-K, Dhbaibi K, Jean M, Dziurka M, Favereau L, Vanthuyne N, Toupet L, Jamoussi B, Srebro-Hooper M, Crassous J (2019) Bis-4-aza[6]helicene: a bis-helicenic 2,2′-bipyridine with chemically-triggered chiroptical switching activity. J Org Chem 84:5383–5393
71. Lee J, Chen H-F, Batagoda T, Coburn C, Djurovich PI, Thompson ME, Forrest SR (2016) Deep blue phosphorescent organic light-emitting diodes with very high brightness and efficiency. Nat Mater 15:92–98
72. Macé A, Hellou N, Hammoud J, Martin C, Gauthier ES, Favereau L, Roisnel T, Caytan E, Nasser G, Vanthuyne N, Williams JAG, Berrée F, Carboni B, Crassous J (2019) An enantiopure cyclometallated iridium complex displaying long-lived phosphorescence both in solution and in the solid state. Helv Chim Acta 102:e1900044
73. Isla H, Crassous J (2016) Helicene-based chiroptical switches. C R Chim 19:39–49
74. Brandt JR, Salerno F, Fuchter MJ (2017) The added value of small-molecule chirality in technological applications. Nat Rev Chem 1:0045
75. Brandt JR, Wang X, Yang Y, Campbell AJ, Fuchter MJ (2016) Circularly polarized phosphorescent electroluminescence with a high dissymmetry factor from PHOLEDs based on a platinahelicene. J Am Chem Soc 138:9743–9746